



Model and proxy evidence for coordinated changes in the hydroclimate of distant regions over the Last Millennium

Pedro José Roldán-Gómez¹, Jesús Fidel González-Rouco¹, Jason E. Smerdon², and Félix García-Pereira¹

¹Instituto de Geociencias, Consejo Superior de Investigaciones Científicas - Universidad Complutense de Madrid, 28040 Madrid, Spain

²Lamont-Doherty Earth Observatory of Columbia University, Palisades, NY, United States of America

Correspondence: P. J. Roldán-Gómez (peroldan@ucm.es)

Abstract. The Medieval Climate Anomaly (MCA; ca. 950-1250 CE) and the Little Ice Age (LIA; ca. 1450-1850 CE) periods, generally characterised by respectively higher and lower temperatures in many regions, have also been associated with drier and wetter conditions in areas around the Intertropical Convergence Zone (ITCZ), the Asian Monsoon region, and in areas impacted by large-scale climatic modes like the Northern and Southern Annular Modes (NAM and SAM, respectively). To analyse coordinated changes in large-scale hydroclimate patterns, and whether similar changes also extend to other periods of the Last Millennium (LM) outside the MCA and the LIA, reconstruction-based products have been analysed, including the collection of tree-ring based Drought Atlases (DA), the Paleo Hydrodynamics Data Assimilation product (PHYDA) and the Last Millennium Reanalysis (LMR). These analyses have shown coherent changes in the hydroclimate of tropical and extratropical regions, such as northern and central South America, East Africa, western North America, Western Europe, the Middle East, Southeast Asia and the Indo-Pacific, during the MCA, the LIA and other periods of the LM. Comparisons with model simulations from the Community Earth System Model - Last Millennium Ensemble (CESM-LME) and phases 5 and 6 of the Coupled Model Intercomparison Project (CMIP5 and CMIP6) show that both external forcing and internal variability contributed to these changes, with the contribution of internal variability being particularly important in the Indo-Pacific basin and that of external forcing in the Atlantic basin. These results may help to identify not only those areas showing coordinated changes, but also those regions where model simulations are able to successfully reproduce the evolution of hydroclimate during the LM.

1 Introduction

The climate of the Last Millennium (LM) was characterised in many regions by periods of warmer and cooler conditions with respect to the pre-industrial mean climate (Diaz et al., 2011; Graham et al., 2010), two well-known examples being the Medieval Climate Anomaly (MCA; ca. 950-1250 CE) and the Little Ice Age (LIA; ca. 1450-1850 CE; Graham et al., 2007; Laird et al., 2012; Ledru et al., 2013). Such temperature changes are often associated with changes in external forcing factors like solar variability and volcanic activity (Mann et al., 2009; Schurer et al., 2013; Fernández-Donado et al., 2013). The impact of these changes on hydroclimate is not straightforward, but reconstructions show that episodes of severe drought also took place during the LM in many regions (Cook et al., 2022). Periods of wetter and drier conditions existed in large areas of North

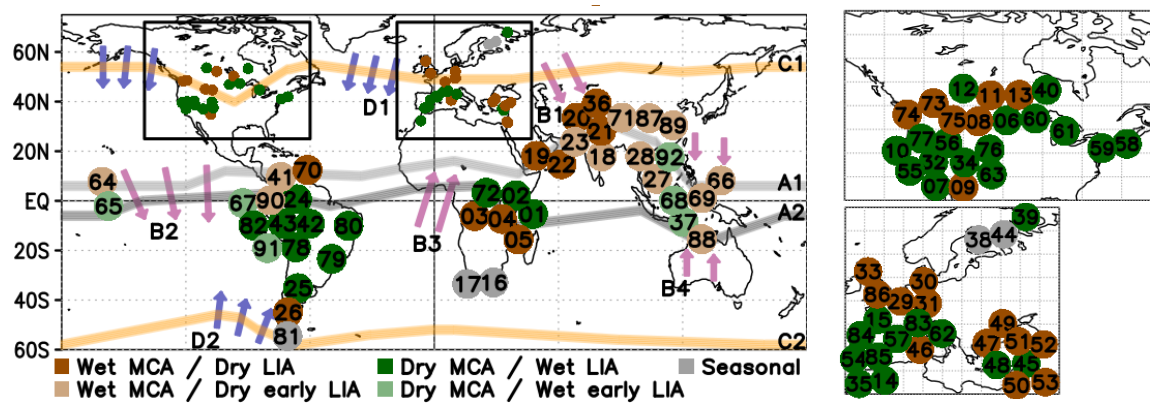


Figure 1. Hydroclimate reconstructions showing (dark brown) drier conditions during MCA and wetter conditions during LIA, (light brown) drier conditions during MCA and wetter conditions during early LIA (until late 1500s CE), (dark green) wetter conditions during MCA and drier conditions during LIA, (light green) wetter conditions during MCA and drier conditions during early LIA (until late 1500s CE), and (gray) drier or wetter conditions in MCA and LIA depending on the season. Detailed references are included in Table 1. As per references of Table 2, A1 and A2 respectively indicate the current position of the ITCZ in July and January, B1 to B4 the ITCZ changes in the transition from MCA to LIA, C1 and C2 the boundary between low and high pressures in the pattern of NAM and SAM, and D1 and D2 the changes in this boundary in the transition from MCA to LIA. Regional maps over North America and Europe are shown on the right side of the panel.

25 America (Cook et al., 2010b), Europe (Luterbacher et al., 2012), South America (Vuille et al., 2012) and Monsoon Asia (Hu et al., 2008), with occurrences that coincide with the MCA and the LIA.

To survey the available evidence, we assessed 92 reconstructions reporting changes from wetter to drier or from drier to wetter conditions during the transition from the MCA to LIA (Fig. 1, with detailed references in Table 1). Some of these reconstructions show consistent drier or wetter conditions during the whole LIA (dark green and dark brown), while others show drier or wetter conditions until late 1500s CE, during the early LIA (light green and light brown), as reported for areas of Pakistan, western India and southern China by Graham et al. (2010). These similarities in the evolution of the hydroclimate of distant regions suggest coordinated changes at a global scale (Graham et al., 2010; Atwood et al., 2021). For example, reconstructions from southwestern North America (Graham et al., 2007; Meko et al., 2001; Cook et al., 2004, 2010b; Hughes and Funkhouser, 1998; Anderson, 2011) and the Mediterranean basin (Luterbacher et al., 2012; Martín-Puertas et al., 2010; Morellón et al., 2009) show drier conditions during the MCA and wetter conditions during the LIA, while reconstructions from northwestern North America (Steinman et al., 2013; Stevens and Dean, 2008), central Europe (Büntgen et al., 2010, 2011) and the British Isles (Wilson et al., 2012; Proctor et al., 2000) tend to show wetter conditions during the MCA and drier conditions during the LIA.

An antiphased relationship between the MCA and LIA is also observed in tropical areas of South America, with wetter conditions during the MCA in areas of northern South America, like the Cariaco Basin in Venezuela (Haug et al., 2001),



Table 1. Location, references and type of reconstruction (sediments, tree rings, speleothems, documentary, ice cores or multi-proxy) for the reconstructions represented in Fig. 1. The first column indicates the code used in Fig. 1 for each reconstruction.

Code	Location	References	Type
01	Lake Challa (Tanzania)	Verschuren et al. (2009); Wolff et al. (2011)	Sediments
02	Lake Naivasha (Kenya)	Verschuren et al. (2000); Verschuren (2001)	Sediments
03	Lake Tanganyika (Tanzania, DRC)	Tierney et al. (2010a)	Sediments
04	Lake Masoko (Tanzania)	Gilbert et al. (2002); Garcin et al. (2006, 2007)	Sediments
05	Lake Malawi (Malawi)	Johnson et al. (2001); Brown and Johnson (2005); Johnson and McCave (2008)	Sediments
06	Moon Lake (North Dakota, USA)	Laird et al. (1996)	Sediments
07	California (USA)	Graham et al. (2007)	Multi-proxy
08	Bighorn (Wyoming, USA)	Gray et al. (2004)	Tree rings
09	Malpais (New Mexico, USA)	Grissino-Mayer (1995)	Tree rings
10	Sacramento River (California, USA)	Meko et al. (2001)	Tree rings
11	Humboldt Lake (Canada)	Michels et al. (2007)	Sediments
12	North Saskatchewan River (Canada)	Case and MacDonald (2003)	Tree rings
13	Red River (Canada)	St.George and Nielsen (2002)	Tree rings
14	Guadalentín River (Spain)	Benito et al. (2010)	Sediments
15	Gardon River (France)	Sheffer et al. (2007)	Sediments
16	Orange River (South Africa)	Tyson and Lindsay (1992)	Sediments
17	Buffels River (W South Africa)	Benito et al. (2011)	Sediments
18	Dandak Cave (India)	Sinha et al. (2007); Berkelhammer et al. (2010)	Speleothems
19	S Oman	Burns et al. (2002)	Speleothems
20	Lunkaransar Lake (India)	Bryson and Swain (1981)	Sediments
21	Pindar Valley (India)	Phadtare and Pant (2006)	Sediments
22	Arabian Sea (Oman)	Anderson et al. (2002); Gupta et al. (2003)	Sediments
23	Karachi (Pakistan)	von Rad et al. (1999)	Sediments
24	Lake Pumacocha (Peru)	Bird et al. (2011)	Sediments
25	N Argentina	Boucher et al. (2011)	Multi-proxy
26	Patagonia	Boucher et al. (2011)	Multi-proxy
27	S Vietnam	Buckley et al. (2010)	Tree rings
28	NW Thailand	Buckley et al. (2007)	Tree rings
29	NE France	Büntgen et al. (2011)	Tree rings
30	N Germany	Büntgen et al. (2010, 2011)	Tree rings



Code	Location	References	Type
31	S Germany	Büntgen et al. (2010, 2011)	Tree rings
32	SW North America	Cook et al. (2004, 2010b)	Tree rings
33	Uamh Cave (NW Scotland)	Proctor et al. (2000)	Speleothems
34	Arizona and Utah (USA)	Ely et al. (1993)	Sediments
35	Morocco	Esper et al. (2007)	Tree rings
36	Karakorum Mountains (Pakistan)	Treydte et al. (2006)	Tree rings
37	Liang Luar Cave (Indonesia)	Griffiths et al. (2016)	Speleothems
38	Finland	Helama et al. (2009)	Tree rings
39	Kola Peninsula (Russia)	Kremenetski et al. (2004)	Multi-proxy
40	NW Ontario (Canada)	Laird et al. (2012)	Sediments
41	Papallacta (Ecuador)	Ledru et al. (2013)	Sediments
42	Marcacocha (S Peru)	Chepstow-Lusty et al. (2009)	Sediments
43	Cascayunga (Peru)	Reuter et al. (2009)	Speleothems
44	Saavajoki River (Finland)	Luoto et al. (2013)	Sediments
45	Antalya and Mersin (SW Turkey)	Touchan et al. (2007)	Tree rings
46	Grotta Verde (Italy)	Antonioli et al. (2003)	Speleothems
47	Urzuntala Cave (NW Turkey)	Göktürk (2011)	Speleothems
48	Kocain Cave (S Turkey)	Göktürk (2011)	Speleothems
49	Sofular Cave (N Turkey)	Göktürk et al. (2011)	Speleothems
50	Nahal Zin (Israel)	Greenbaum et al. (2000)	Sediments
51	Nar Gölü (C Turkey)	Jones et al. (2006); Woodbridge and Roberts (2011)	Sediments
52	Tercer Lake (C Turkey)	Kuzucuoglu et al. (2011)	Sediments
53	Dead Sea	Bookman et al. (2004); Neumann et al. (2007)	Sediments
54	Zoñar Lake (S Spain)	Martín-Puertas et al. (2008, 2010)	Sediments
55	Sierra Nevada (California, USA)	Stine (1994)	Tree rings
56	Great Basin (W North America)	Hughes and Funkhouser (1998)	Tree rings
57	NE Spain	Llasat et al. (2003)	Documentary
58	Little Pond (Massachusetts, USA)	Oswald and Foster (2011)	Sediments
59	Piermont Marsh (New York, USA)	Pederson et al. (2005)	Sediments
60	Hole Bog (Minnesota, USA)	Booth et al. (2006)	Sediments
61	Minden Bog (Michigan, USA)	Booth et al. (2006)	Sediments
62	Lake Accesa (Italy)	Magny et al. (2007)	Sediments
63	San Juan Mountains (Colorado, USA)	Routson et al. (2011)	Tree rings
64	Teraina (Kiribati)	Sachs et al. (2009)	Sediments



Code	Location	References	Type
65	Kiritimati (Kiribati)	Sachs et al. (2009); Higley et al. (2018)	Sediments
66	Mecherchar Island (Palau)	Sachs et al. (2009)	Sediments
67	San Cristóbal Island (Ecuador)	Sachs et al. (2009)	Sediments
68	Makassar Strait (Indonesia)	Newton et al. (2006); Tierney et al. (2010b)	Sediments
69	Kau Bay (Indonesia)	Langton et al. (2008)	Sediments
70	Cariaco Basin (Venezuela)	Haug et al. (2001)	Sediments
71	Dongge Cave (S China)	Wang et al. (2005)	Speleothems
72	Lake Victoria (Tanzania, Uganda, Kenya)	Stager et al. (2005)	Sediments
73	Castor Lake (Washington, USA)	Steinman et al. (2013)	Sediments
74	Lime Lake (Washington, USA)	Steinman et al. (2013)	Sediments
75	Crevice Lake (Montana, USA)	Stevens and Dean (2008)	Sediments
76	Bison Lake (Colorado, USA)	Anderson (2011)	Sediments
77	Pyramid Lake (Nevada, USA)	Benson et al. (2002)	Sediments
78	Quelccaya Ice Cap (Peru)	Vuille et al. (2012); Thompson et al. (1986)	Ice cores
79	Cristal Cave (SE Brazil)	Vuille et al. (2012); Taylor (2010)	Speleothems
80	Diva & Torrinha Caves (NE Brazil)	Vuille et al. (2012); Novello et al. (2012)	Speleothems
81	S South America	Neukom et al. (2010)	Multi-proxy
82	Palestina Cave (NW Peru)	Apaéstegui et al. (2014)	Speleothems
83	Lake Allos (France)	Wilhelm et al. (2012)	Sediments
84	Lake Taravilla (Spain)	Moreno et al. (2008)	Sediments
85	Lake Estanya (NE Spain)	Morellón et al. (2009, 2011)	Sediments
86	SC England	Wilson et al. (2012)	Tree rings
87	Wanxiang Cave (China)	Zhang et al. (2008)	Speleothems
88	Cave KNI-51 (N Australia)	Denniston et al. (2016)	Speleothems
89	Heshang Cave (China)	Hu et al. (2008)	Speleothems
90	Laguna Pallcacocha (S Ecuador)	Moy et al. (2002)	Sediments
91	Peruvian Shelf (Peru)	Rein et al. (2004)	Sediments
92	Dongdao Island (S China Sea)	Yan et al. (2011)	Sediments

and drier conditions in areas of central South America, like Peru (Bird et al., 2011; Reuter et al., 2009; Vuille et al., 2012; Thompson et al., 1986; Apaéstegui et al., 2014) and Eastern Brazil (Vuille et al., 2012; Taylor, 2010; Novello et al., 2012). In East Africa, Anchukaitis and Tierney (2013) showed coordinated changes for lake Challa (Verschuren et al., 2009; Wolff et al., 2011), Naivasha (Verschuren et al., 2000; Verschuren, 2001), Tanganyika (Tierney et al., 2010a), Masoko (Gilbert et al., 2002; 45 Garcin et al., 2006, 2007) and Malawi (Johnson et al., 2001; Brown and Johnson, 2005; Johnson and McCave, 2008), with an opposite behavior between the lakes in the south and the north of the Intertropical Convergence Zone (ITCZ). Changes in



Table 2. References for the position of ITCZ, the boundary between low and high pressures in the pattern of NAM and SAM, and the changes in these two elements during MCA and LIA, according to the codes included in Fig. 1.

Code	Mode	References
A1	Modern position of July ITCZ	Newton et al. (2006)
A2	Modern position of January ITCZ	Newton et al. (2006)
B1	ITCZ changes in the Indian Monsoon region	Fleitmann et al. (2003)
B2	ITCZ changes in the Eastern Pacific	Higley et al. (2018)
B3	ITCZ changes in East Africa	Anchukaitis and Tierney (2013)
B4	ITCZ changes in the Western Pacific	Denniston et al. (2016); Yan et al. (2015)
C1	Boundary of low/high in the pattern of NAM	Li and Wang (2003)
C2	Boundary of low/high in the pattern of SAM	Gong and Wang (1999)
D1	Changes in NAM/NAO	Ortega et al. (2015)
D2	Changes in SAM	Jones et al. (2009); Fogt et al. (2009)

the ITCZ have been also associated with coordinated changes in the hydroclimate of the Indian Monsoon region, with wetter conditions during the MCA and drier conditions during the LIA for wide areas of Pakistan (von Rad et al., 1999; Treydte et al., 2006), India (Sinha et al., 2007; Berkelhammer et al., 2010; Bryson and Swain, 1981; Phadtare and Pant, 2006) and the Arabian Sea (Burns et al., 2002; Fleitmann et al., 2003; Anderson et al., 2002; Gupta et al., 2003). Alterations of the ITCZ have been also associated with changes in the hydroclimate of the Indo-Pacific basin (Atwood et al., 2021), with a marked transition between the MCA and LIA in areas of China (Wang et al., 2005; Zhang et al., 2008; Hu et al., 2008), Southeast Asia (Buckley et al., 2010, 2007), Indonesia (Griffiths et al., 2016; Newton et al., 2006; Tierney et al., 2010b), northern Australia (Denniston et al., 2016) and the eastern Pacific islands (Sachs et al., 2009; Higley et al., 2018).

Most reconstructions in Fig. 1 are located in extratropical areas, in the boundary between low and high pressures within the regions of the Northern and Southern Annular Modes (NAM and SAM; Thompson and Wallace, 2001; Jones et al., 2009; Fogt et al., 2009), or in tropical areas around the ITCZ (Table 2). Analyses based on simulated data (Roldán-Gómez et al., 2020) link transitions from the MCA to LIA in extratropical areas with alterations in the variability of modes like the NAM and SAM (Ortega et al., 2015; Jones et al., 2009; Fogt et al., 2009), mainly driven by changes in external forcing factors (Roldán-Gómez et al., 2020). In tropical areas, the transitions from the MCA to LIA can be linked to alterations of the ITCZ (Atwood et al., 2021), like a contraction over the Western Pacific (Denniston et al., 2016; Yan et al., 2015) and shifts over East Africa (Anchukaitis and Tierney, 2013), the Indian Monsoon region (Fleitmann et al., 2003) and the Eastern Pacific (Higley et al., 2018). The analysis of the simulated hydroclimate from the Community Earth System Model - Last Millennium Ensemble (CESM-LME; Otto-Bliesner et al., 2015) performed by Roldán-Gómez et al. (2022) shows that these alterations of the ITCZ may be impacted by both external forcing factors and internal variability.



Even if individual reconstructions from different regions suggest coordinated changes in the hydroclimate during the MCA and LIA, global analyses based on proxy data are scarce and limited to certain reconstructions and products. The analysis of simulated data provides an insight into the mechanisms explaining coordinated changes in the hydroclimate of the LM, but analyses of LM simulations must account for both forced and internal variability (Roldán-Gómez et al., 2022). This work
70 addresses these challenges by performing a comparative assessment of the LM hydroclimate at global and large-continental scales from different sources, including reconstructions, model simulations, and hybrid products based on data assimilation and reanalysis. The use of several reconstruction-based products allows the identification with a robustness assessment of those regions more impacted by hydroclimatic changes during the MCA and LIA, and more generally during the LM. The comparison between reconstruction-based products and model simulations from different ensembles allows an assessment of
75 the contributions of external forcing and internal variability on the hydroclimate of each region, showing those regions where model simulations can provide representative information about changes in the hydroclimate.

2 Data and methods

The following reconstruction-based products are employed: the 100-member ensemble of the Paleo Hydrodynamics Data Assimilation product (PHYDA; Steiger et al., 2018), the 20-member ensemble of the Last Millennium Reanalysis (LMR; Tardif et al., 2019) and the tree-ring based Drought Atlases (DA), including the Old World Drought Atlas (OWDA; Cook et al., 2015), the North American Drought Atlas (NADA; Cook et al., 2010b), the Monsoon Asia Drought Atlas (MADA; Cook et al., 2010a) and the Mexican Drought Atlas (MXDA; Stahle et al., 2016). Due to the fact that they do not extend back into the MCA, other DAs have not been included in our analyses.
80

Regarding the model-based products, we use the 13 all-forcing simulations of the CESM-LME, together with 10 LM simulations from the Coupled Model Intercomparison Project Phase 5 / Paleoclimate Modelling Intercomparison Project Phase 3 (CMIP5/PMIP3; Taylor et al., 2007; Schmidt et al., 2011, 2012; Stocker et al., 2013) and 4 LM simulations from the Coupled Model Intercomparison Project Phase 6 / Paleoclimate Modelling Intercomparison Project Phase 4 (CMIP6/PMIP4; Eyring et al., 2016; Jungclaus et al., 2017), all of which are described in Table 3. All these simulations have been interpolated to a common grid resolution of 6°x6°, the coarsest among the analysed simulations, to allow for the calculation of ensemble averages across the CESM-LME, CMIP5 and CMIP6 products. The CESM-LME and CMIP5 simulations are forced according to the CMIP5/PMIP3 protocol (Schmidt et al., 2011, 2012), while the CMIP6 simulations consider the CMIP6/PMIP4 protocol (Jungclaus et al., 2017).
90

Considering the wide bibliography of single-point reconstructions showing wetter or drier conditions during MCA and LIA (Fig. 1), most analyses have been based on these two periods. Following the approach of Masson-Delmotte et al. (2013), the MCA has been considered from 950 to 1250 CE, and the LIA from 1450 to 1850 CE, even if these temporal intervals might not be suitable for all the regions and for all products (Neukom et al., 2014, 2019). To assess the robustness of our results to the specifics of this definition, we have performed additional analyses based on the trend during the whole period from 950 to 1750 CE, and report our findings in the Appendix A.
95



Table 3. Reconstruction-based and model products considered in this work. In case of being referred to an ensemble of experiments, the acronym used for the ensemble and the number of members (N) are provided. References describing each product are provided in the last column.

Ensemble	Product/Model	N	References
DA	Old World Drought Atlas (OWDA)	1	Cook et al. (2015)
DA	North American Drought Atlas (NADA)	1	Cook et al. (2010b)
DA	Monsoon Asia Drought Atlas (MADA)	1	Cook et al. (2010a)
DA	Mexican Drought Atlas (MXDA)	1	Stahle et al. (2016)
LMR	Last Millennium Reanalysis (LMR)	20	Tardif et al. (2019)
PHYDA	Paleo Hydrodynamics Data Assimilation (PHYDA)	100	Steiger et al. (2018)
CESM-LME	Community Earth System Model (CESM)	13	Otto-Bliesner et al. (2015)
CMIP5	Goddard Institute for Space Studies (GISS)	3	Schmidt et al. (2006, 2014)
CMIP5	Model for Interdisciplinary Research on Climate (MIROC-ESM)	1	Watanabe et al. (2011)
CMIP5	Hadley Centre Coupled Model (HadCM)	1	Tett et al. (2007)
CMIP5	Community Climate System Model (CCSM)	1	Landrum et al. (2013)
CMIP5	Institut Pierre Simon Laplace (IPSL)	1	Dufresne et al. (2013)
CMIP5	Commonwealth Scientific and Industrial Research Organization (CSIRO)	1	Phipps et al. (2012)
CMIP5	Meteorological Research Institute (MRI)	1	Yukimoto et al. (2011); Adachi et al. (2013)
CMIP5	Max Planck Institut für Meteorologie (MPI)	1	Giorgetta et al. (2013)
CMIP6	MIROC Earth System version 2 for Long-term simulations (MIROC-ES2L)	1	Hajima et al. (2020)
CMIP6	Meteorological Research Institute (MRI)	1	Yukimoto et al. (2019)
CMIP6	Max Planck Institut für Meteorologie (MPI)	2	Mauritsen et al. (2019)



Our analyses focus on reconstructions of the Palmer Drought Severity Index (PDSI; Palmer, 1965). The PDSI is directly
100 provided by the DAs, the PHYDA and the LMR. For the CMIP5, CMIP6 and CESM-LME simulations, PDSI has been com-
puted based on atmospheric variables and soil parameters, following the approach of a self-calibrating PDSI (scPDSI; Wells
et al., 2004). The potential evapotranspiration is calculated using the Thornthwaite's method (Thornthwaite, 1948). While the
Thornthwaite formulation has been shown to have limitations for projections of 21st-century soil moisture conditions because
of its strong dependence on temperature, assessments of the Thornthwaite formulation in model simulations of the LM have
105 shown that such limitations are not a concern for the LM period (Smerdon et al., 2015).

The PHYDA provides water-year annual averages and seasonal averages for the boreal summer (June, July and August; JJA)
and winter (December, January, and February; DJF). The LMR only provides annual averages, while the Northern Hemisphere
DAs exclusively target the JJA period. For all the analyses, JJA values are considered for all the products except for the LMR,
for which the annual values are used. To confirm that the annual results from the LMR can be meaningfully compared to
110 the seasonal results from the other products, the annual PDSI from the PHYDA and the ensembles of CMIP5, CMIP6 and
CESM-LME are analysed in Appendix B.

Coordinated changes during the MCA and the LIA are characterized by computing the difference between each variable and
product during the LIA and MCA periods. The agreement between products is also assessed by computing the global spatial
correlation between PDSI LIA-MCA maps from each product (Coats et al., 2013a), and by counting the number of products
115 showing positive or negative PDSI differences for each location. Finally, time series of PDSI for the whole millennium are
extracted from different locations and different products, to analyse the correlations between them beyond the periods of the
MCA and LIA.

3 Results

3.1 Reconstructions of hydroclimate during the MCA and LIA

120 PDSI differences between the LIA and MCA are shown for the DAs, the PHYDA and the LMR (Fig. 2). Some wetting and
drying patterns are consistent across the DAs (Fig. 2a), the PHYDA (Fig. 2b), and the LMR (Fig. 2c). For example, all products
estimate drier conditions during the LIA and wetter conditions during the MCA over the Middle East. In the PHYDA and LMR
these conditions are associated with a warmer LIA in these regions (Fig. 3). There is also good agreement across the PHYDA
and LMR in South America, with drier conditions in the north and wetter conditions in the central continent during the LIA,
125 as well as in northern Canada, Scandinavia and northern Eurasia, with wetter conditions during the LIA, associated all of
them with lower temperatures (Fig. 3). The PHYDA and the LMR agree well with the reconstructions of Fig. 1, which also
show drier conditions during the LIA in southeastern Europe and Anatolia (Göktürk, 2011; Jones et al., 2006; Woodbridge and
Roberts, 2011; Kuzucuoglu et al., 2011), the Indian Monsoon region (Burns et al., 2002; Bryson and Swain, 1981; Phadtare
and Pant, 2006; Anderson et al., 2002; Gupta et al., 2003) and South America north of the ITCZ (Haug et al., 2001). The LMR
130 also agree with the reconstructions of Fig. 1 in regions of East Africa (Anchukaitis and Tierney, 2013).

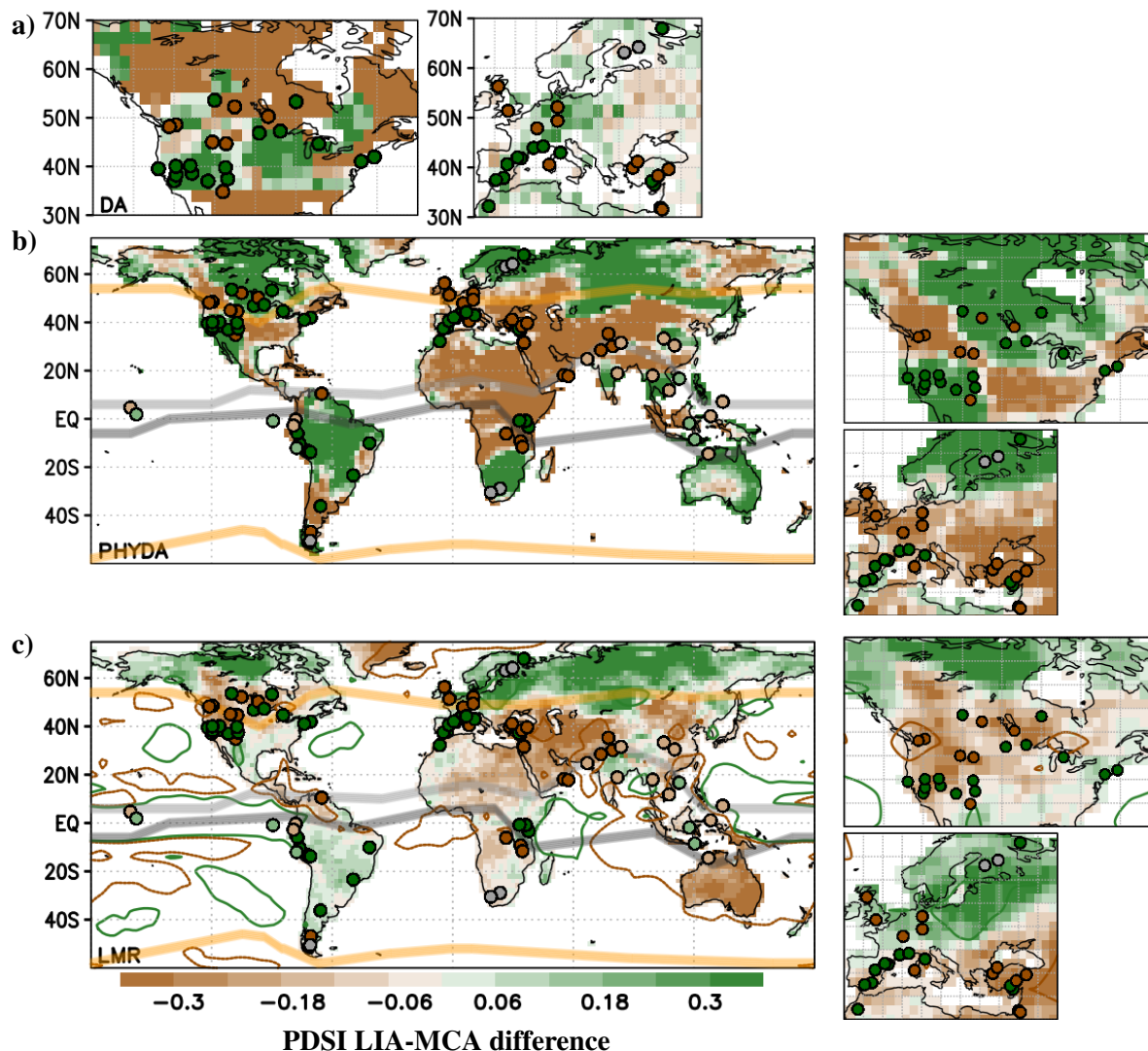


Figure 2. LIA-MCA differences in PDSI (shading) or precipitation (contours) from (a) DAs, (b) PHYDA, and (c) LMR. Dots represent the locations of Fig. 1, with the same color code considered in that figure; positions of the modern ITCZ and NAM and SAM boundaries are also shown, as described in Fig. 1. For the precipitation, contours of -1 (brown) and 1 (green) mm/month are shown. Average of JJA is considered for the PHYDA and the DAs, while the annual average is considered for the LMR. For the PHYDA and the LMR, regional maps over North America and Europe are shown on the right side of each corresponding panel.

In western North America there is a good agreement between the DA and PHYDA, and between these two products and the reconstructions of Fig. 1, most of them showing wetter conditions in the southwest and drier conditions in the northwest during the LIA (Steinman et al., 2013; Cook et al., 2004, 2010b). Each of these products are nevertheless in contrast to the LMR, which shows drier conditions during the LIA for most of the American West, in sharp contrast with a broad range of literature

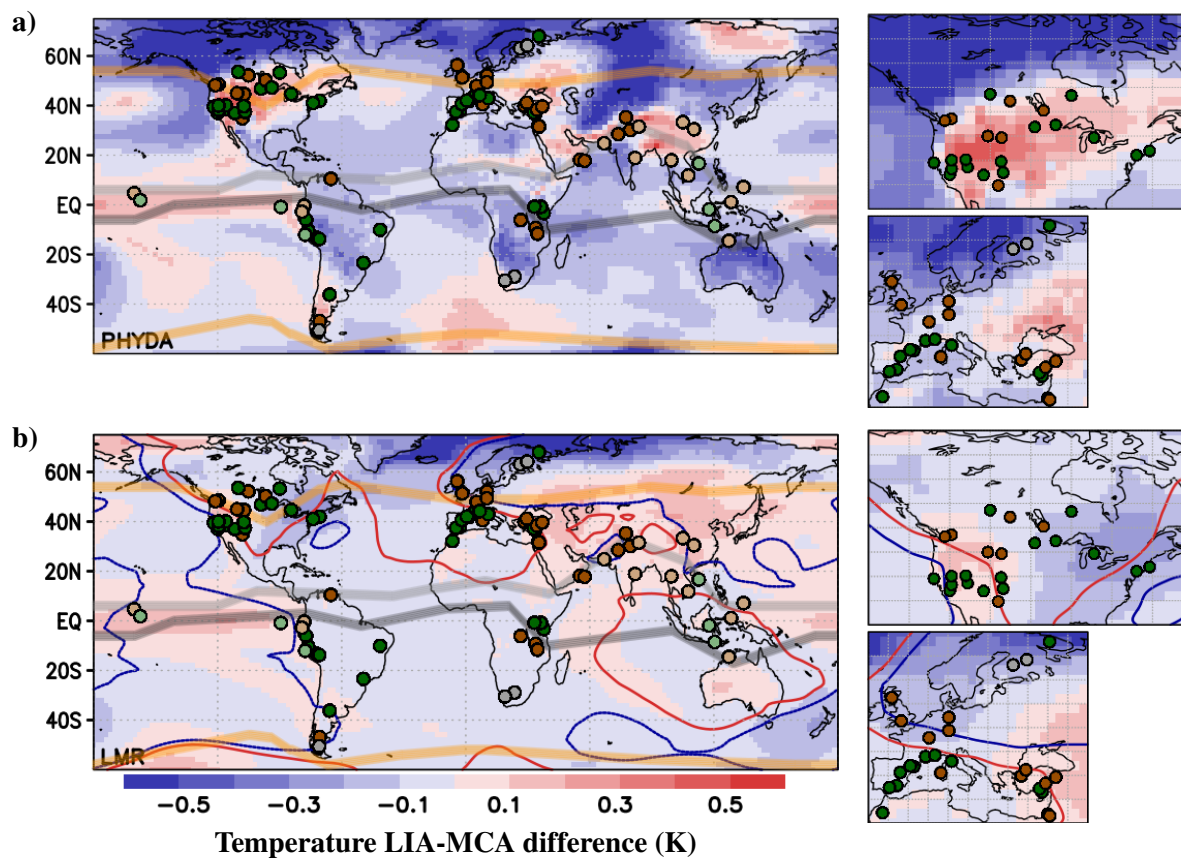


Figure 3. LIA-MCA differences in temperature from (a) PHYDA, and (b) LMR. Dots represent the locations of Fig. 1, with the same color code considered in that figure; positions of the modern ITCZ and NAM and SAM boundaries are also shown, as described in Fig. 1. For the LMR, differences in SLP are also shown with contours of -5 (blue) and 5 (red) Pa. Average of JJA is considered for the PHYDA, while the annual average is considered for the LMR. For each product, regional maps over North America and Europe are shown on the right side of each corresponding panel.

135 on megadroughts during the MCA period (Cook et al., 2010b; Coats et al., 2013b). For the case of central and western Europe,
the PHYDA estimates drier conditions during the LIA, in agreement with the reconstructions of Fig. 1 (Luterbacher et al.,
2012), while the DA and LMR estimate wetter conditions. Differences between products are particularly relevant in the Indo-
Pacific basin, where the PHYDA and LMR show opposite behavior in Australia, Southeast Asia and Patagonia, and in high
latitudes, with opposite behavior in areas of Alaska and northeast Asia. These differences coincide with opposite estimates
140 in temperature differences as well, with the PHYDA (Fig. 3a) and LMR (Fig. 3b) respectively showing warmer or cooler
conditions in Patagonia and cooler or warmer conditions in Australia during the LIA.

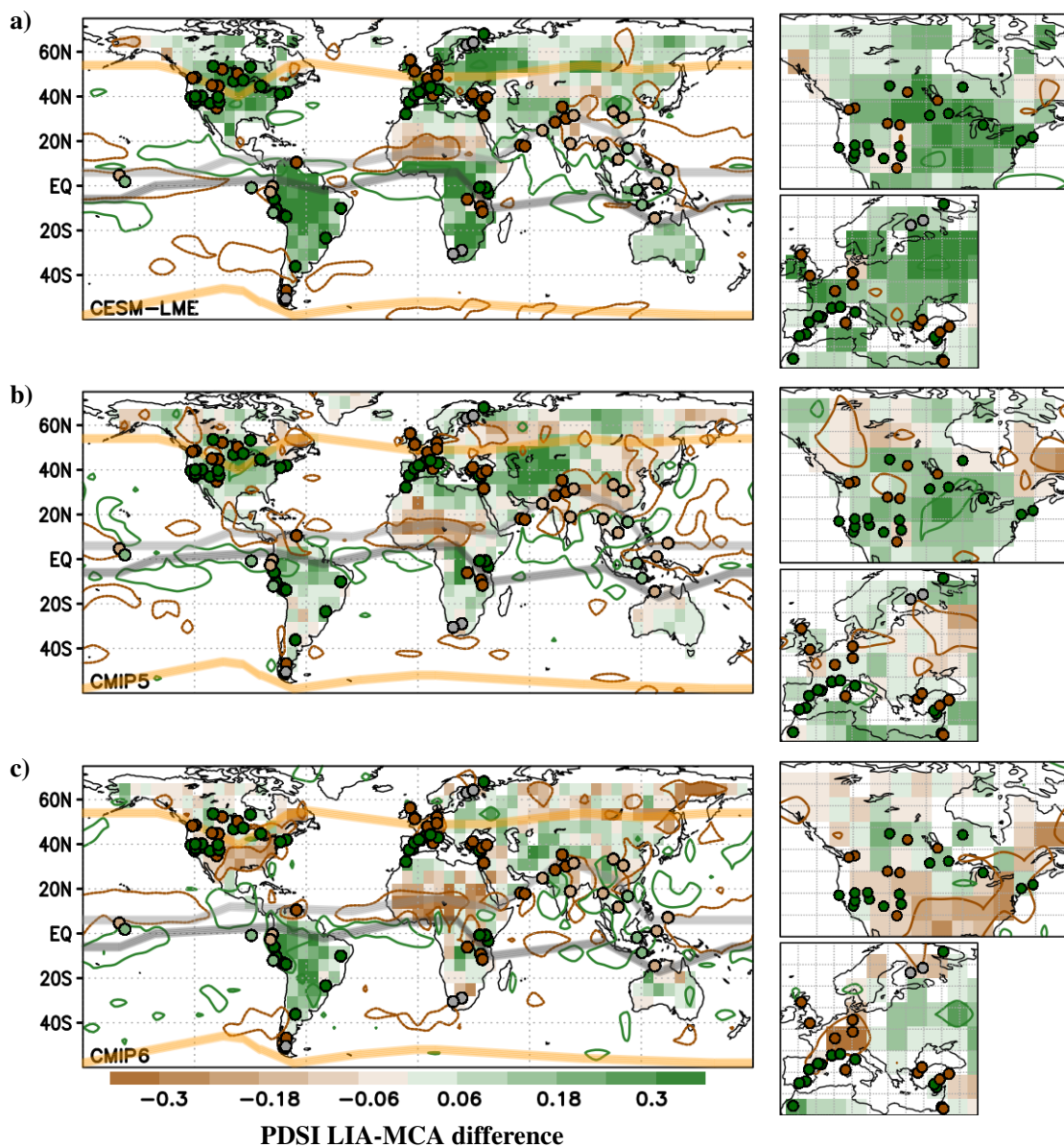


Figure 4. LIA-MCA differences in PDSI (shading) or precipitation (contours) from the ensemble average of (a) CESM-LME, (b) CMIP5 and (c) CMIP6 LM simulations. Dots represent the locations of Fig. 1, with the same color code considered in that figure; positions of the modern ITCZ and NAM and SAM boundaries are also shown, as described in Fig. 1. For the precipitation, contours of -1 (brown) and 1 (green) mm/month are shown. In all the cases, average of JJA is considered. For each product, regional maps over North America and Europe are shown on the right side of each corresponding panel.

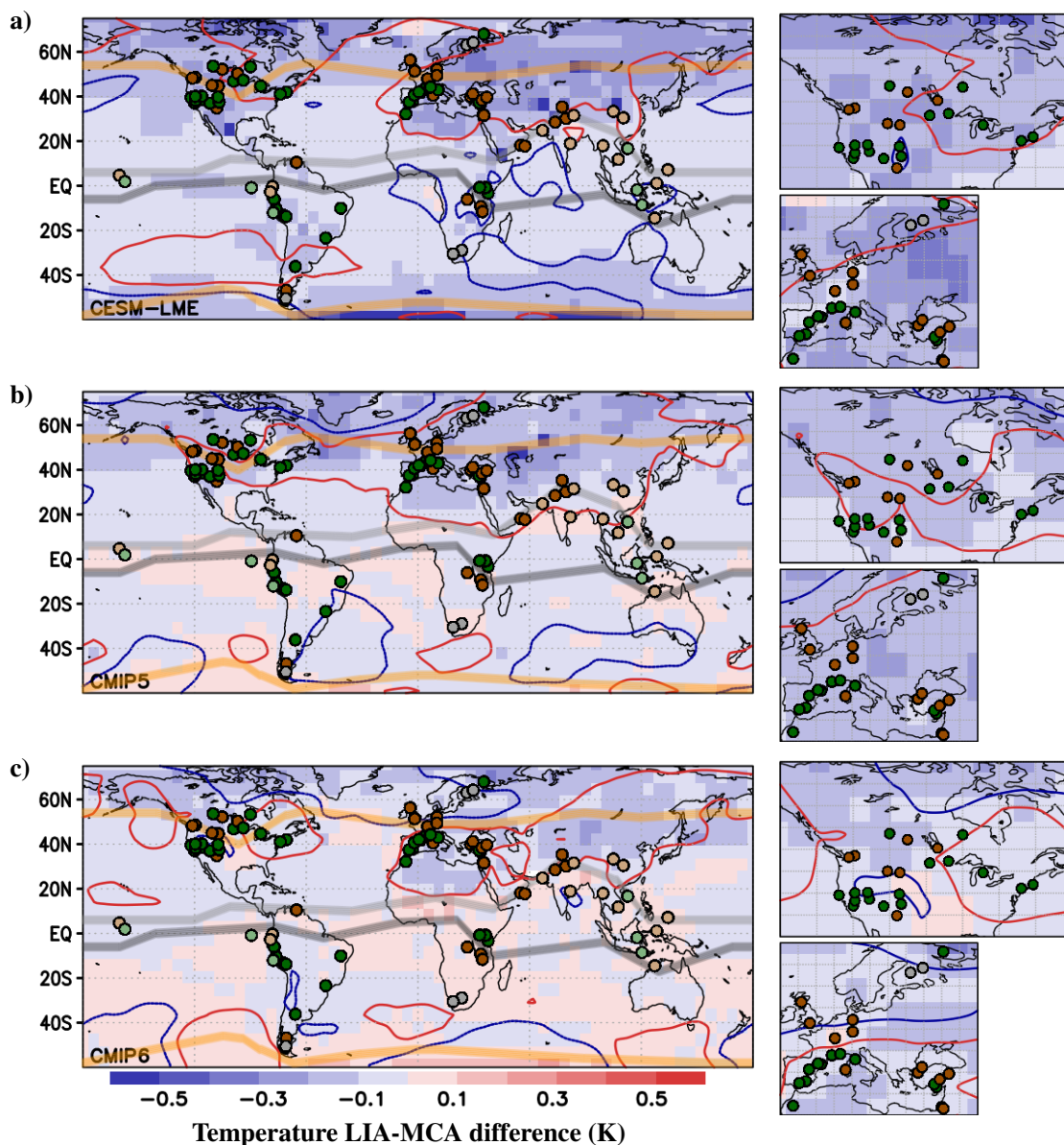


Figure 5. LIA-MCA differences in temperature (shading) or SLP (contours) from the ensemble average of (a) CESM-LME, (b) CMIP5 and (c) CMIP6 LM simulations. Dots represent the locations of Fig. 1, with the same color code considered in that figure; positions of the modern ITCZ and NAM and SAM boundaries are also shown, as described in Fig. 1. For the SLP, contours of -5 (blue) and 5 (red) Pa are shown. In all the cases, average of JJA is considered. For each product, regional maps over North America and Europe are shown on the right side of each corresponding panel.

3.2 Simulated hydroclimate during the MCA and LIA

The analysis of the model ensembles allows an estimate of those areas that are potentially more impacted by external forcing as estimated by the models, because individual simulations include different realisations of internal variability but share the external forcing changes imposed as boundary conditions (Fernández-Donado et al., 2013; Jungclaus et al., 2017).



Figure 4 shows the mean PDSI differences between the LIA and MCA for the CESM-LME, CMIP5 and CMIP6 LM ensembles. For the areas of the Middle East and southern Asia the agreement between the DAs, the PHYDA, the LMR and the reconstructions of Fig. 1 extends also to the simulations from CESM-LME (Fig. 4a), CMIP5 (Fig. 4b) and CMIP6 (Fig. 4c). There is also a good agreement in central South America, where the CESM-LME (Fig. 4a), CMIP5 (Fig. 4b) and CMIP6 (Fig. 4c) simulations all show a wet LIA for the areas south of the ITCZ, also linked to cooler temperatures during this period (Fig. 5). For northern South America, the dry LIA observed in reconstructions (Fig. 2b,c) is also found, with a limited extension, in CMIP5 (Fig. 4b) and CMIP6 (Fig. 4c) simulations. The agreement found for these areas is consistent with an impact of external forcing on the position of the Atlantic ITCZ (Roldán-Gómez et al., 2022) and the intensity of the monsoon system (Roldán-Gómez et al., 2020).

In western North America and Western Europe, the CMIP5 simulations (Fig. 4b) show a good agreement with the reconstructions of Fig. 1 and with the PHYDA (Fig. 2b). However, this consistency is not so clear in the simulations from CMIP6 (Fig. 4c), for which a dry LIA is found in most regions of North America, associated with limited cooling during that period (Fig. 5c). Disagreement also exists in the CESM-LME (Fig. 4a), which simulates a dry LIA in some areas of southwestern North America and a wet LIA in Western and Northern Europe. These differences can be linked to different atmospheric dynamics, with the CMIP5 ensemble showing important differences in sea level pressure (SLP) between the MCA and the LIA in most regions of North America and Europe, while the CMIP6 ensemble and the CESM-LME limit these changes to some areas of Southern and Eastern Europe and northern North America. Despite these differences, all the models show relevant changes in these regions during the MCA and LIA, in line with the changes in the North Atlantic Oscillation (NAO) shown in Roldán-Gómez et al. (2020).

In the Indo-Pacific basin, the ensemble average of CESM-LME (Fig. 4a), CMIP5 (Fig. 4b) and CMIP6 (Fig. 4c) LM simulations show small PDSI differences between the MCA and LIA, with no clear agreement with the PHYDA (Fig. 2b) and the LMR (Fig. 2c). The CESM-LME (Fig. 5a) tends to show cooler conditions during the LIA in these regions, but the temperature difference is small compared to that of North America and Europe. For the case of CMIP5 (Fig. 5b) and CMIP6 (Fig. 5c), warmer conditions are found during the LIA for some areas of India and northern Australia. Regarding the atmospheric dynamics, only the LMR shows relevant changes in SLP for the Indo-Pacific, with positive anomalies in the Indian and western Pacific basin and negative anomalies in the eastern Pacific basin during the LIA. This behavior is consistent with a larger impact of internal variability in these areas (Roldán-Gómez et al., 2022), with simulation-dependent changes that are filtered out when working with ensemble averages.

3.3 Agreement between products

To assess the agreement between different pairs of products, spatial pattern correlations for the global maps of Fig. 2 and Fig. 4 have been included in Table 4. Despite the regional differences found in areas of North America and the Indo-Pacific basin, the ensembles of CESM-LME, CMIP5 and CMIP6 show global spatial correlations between 0.29 and 0.39. The global correlation of reconstruction-based products is strongly impacted by low correlations in some areas of the southern hemisphere and at high latitudes, with a lower density of proxy data. If these regions are excluded (Table 5), correlations larger than 0.29



Table 4. Correlation between the maps of differences LIA-MCA of PDSI from DAs (Fig. 2a), PHYDA (Fig. 2b), LMR (Fig. 2c), CESM-LME (Fig. 4a), CMIP5 (Fig. 4b) and CMIP6 (Fig. 4c). Significant correlations ($p < 0.05$) accounting for autocorrelation are shown in bold.

	PHYDA	LMR	CESM	CMIP5	CMIP6
DAs	-0.05	-0.06	-0.11	0.08	-0.08
PHYDA		0.32	0.24	0.10	0.18
LMR			0.05	-0.08	0.05
CESM				0.33	0.29
CMIP5					0.39

Table 5. Same as Table 4, but considering only the data between 20°S and 50°N.

	PHYDA	LMR	CESM	CMIP5	CMIP6
DAs	0.35	-0.08	-0.04	0.30	0.08
PHYDA		0.29	0.35	0.11	0.27
LMR			0.24	-0.10	0.16
CESM				0.36	0.32
CMIP5					0.45

180 are also found between DAs and PHYDA and between PHYDA and LMR. The disagreement between LMR and the other reconstruction-based products in areas of Western Europe and western North America explains the small global correlation between the DAs and LMR. It is important to note that the spatial correlation between reconstruction-based and model-based products is impacted by internal variability. The use of ensemble averages removes the contribution of internal variability as it was manifest in the climate trajectory from the simulated data. For the reconstruction-based products the contribution of
 185 internal variability is not removed, even if the multi-century averages for the LIA and MCA periods emphasize the contribution of the external forcing.

The agreement between sources is particularly poor in areas of the Indo-Pacific basin. As shown in Fig. 6a, there is no clear agreement regarding the sign of the PDSI LIA-MCA differences for areas of Southeast Asia and Australia. There is also no clear agreement for these areas among the individual simulations comprising the CMIP5 and CMIP6 ensembles (Fig. 6b),
 190 suggesting that the hydroclimate of these areas is strongly impacted by simulation-dependent processes, likely those associated with internal variability. These results are in line with the results obtained with the CESM-LME by Roldán-Gómez et al. (2022), showing a relevant impact of internal variability on the position and extension of the Indian and western Pacific ITCZ.

In other areas, most products (Fig. 6a) and most individual simulations (Fig. 6b) show the same sign of PDSI differences such as in central South America, with a drier MCA and a wetter LIA, or the Sahel, extending from Western Africa to the

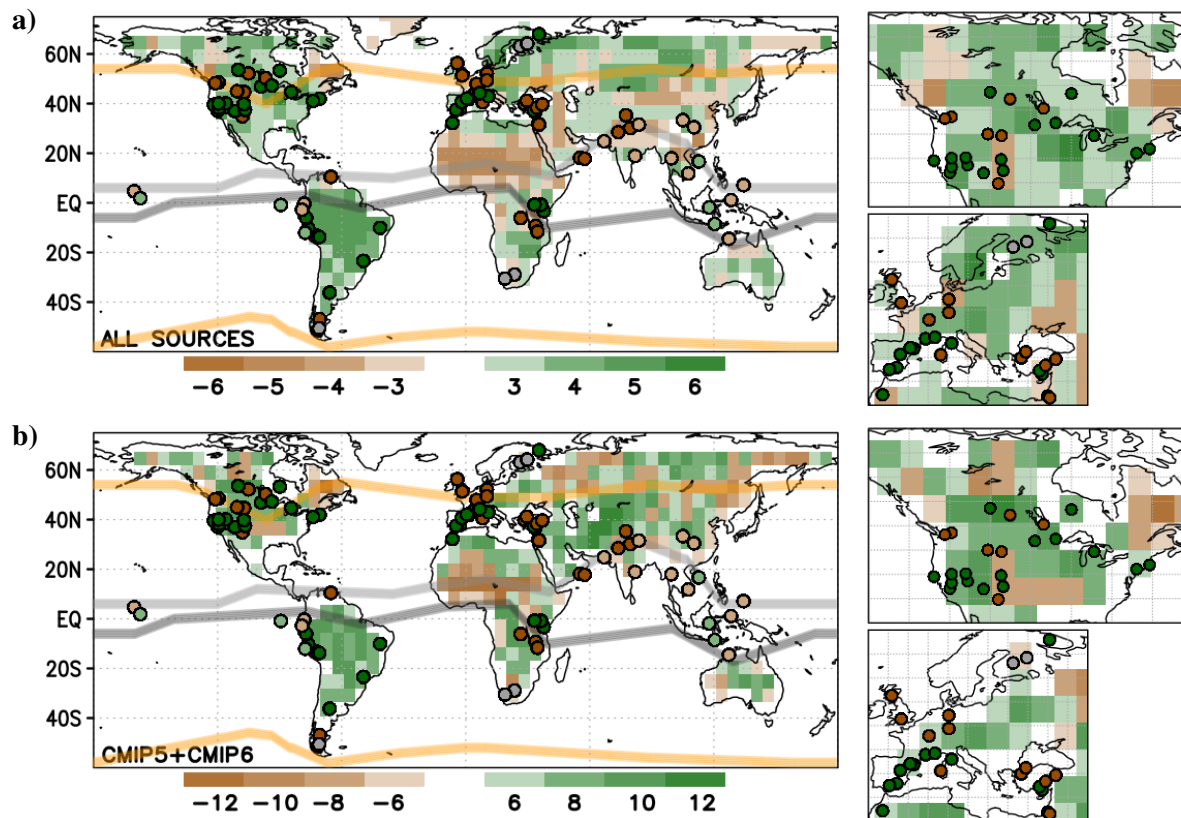


Figure 6. (a) Number of products, from DAs, PHYDA, LMR, and the ensemble averages of CESM-LME, CMIP5 and CMIP6, showing positive (green) or negative (brown) PDSI differences LIA-MCA. (b) Number of simulations, from the ensembles of CMIP5 and CMIP6, showing positive (green) or negative (brown) PDSI differences LIA-MCA. Dots represent the locations of Fig. 1, with the same color code considered in that figure; positions of the modern ITCZ and NAM and SAM boundaries are also shown, as described in Fig. 1. Regional maps over North America and Europe are shown on the right side of each corresponding panel.

195 Arabian peninsula, for which most products and simulations show a wetter MCA and a drier LIA. Consistency also extends to areas of western North America, with at least 4 products showing wetter conditions in the south and drier conditions in the north during the LIA, or to northern India, where most products show a wetter MCA and a drier LIA. The agreement for these areas suggest a contribution of external forcing that is more important than that of internal variability.

200 The MCA and the LIA are periods extensively addressed in the literature, but they are not the only periods showing relevant droughts (Cook et al., 2022). The analyses have been then extended to other periods, by extracting time series of PDSI for the whole millennium from the same regions that show coordinated changes during the MCA and LIA (Fig. 7a-e and 8a-e), including western North America, southwestern Europe, northern and central South America, East Africa, Pakistan, India, Southeast Asia and Indonesia. For each region, the correlations between the DAs, the PHYDA, the LMR, and the ensemble average of CESM-LME, CMIP5 and CMIP6 LM simulations have been computed (Fig. 7f-j and 8f-j).

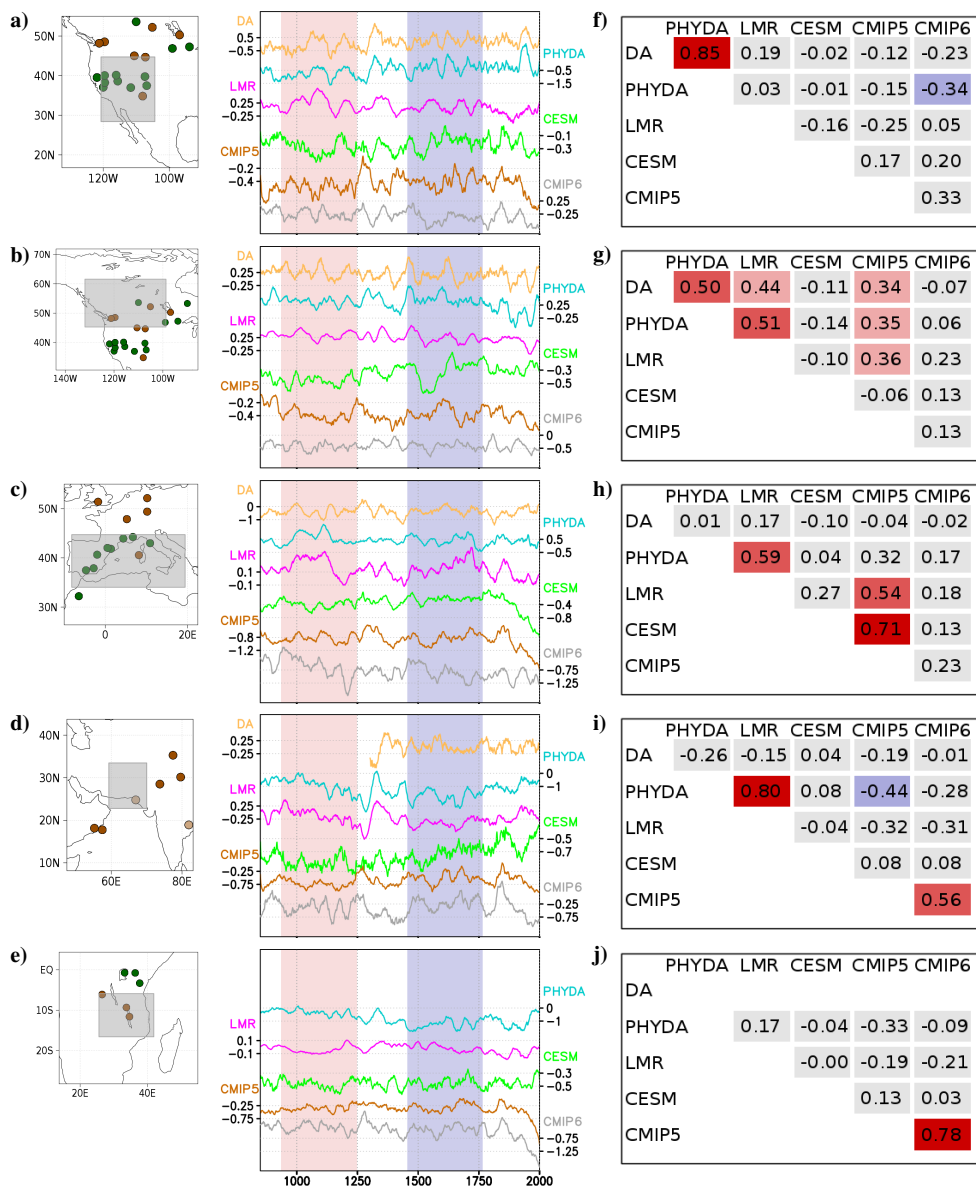


Figure 7. (a-e) Time series of PDSI for (a) southwestern North America, (b) northwestern North America, (c) southwestern Europe, (d) Pakistan and (e) East Africa, obtained from DAs, PHYDA, LMR, and the ensemble average of CESM-LME, CMIP5, and CMIP6 LM simulations. Time series of DAs are not available for those regions not considered in OWDA, NADA, MADA and MXDA. Periods of MCA and LIA are highlighted in red and blue in the middle panels. Dots in the map of the left side represent the locations of Fig. 1, with the same color code considered in that figure. (f-j) Correlations between time series of PDSI for each region obtained from DAs, PHYDA, LMR, and the ensemble average of CESM-LME, CMIP5, and CMIP6 LM simulations. Color code for the correlations is the same as included in Fig. 9.

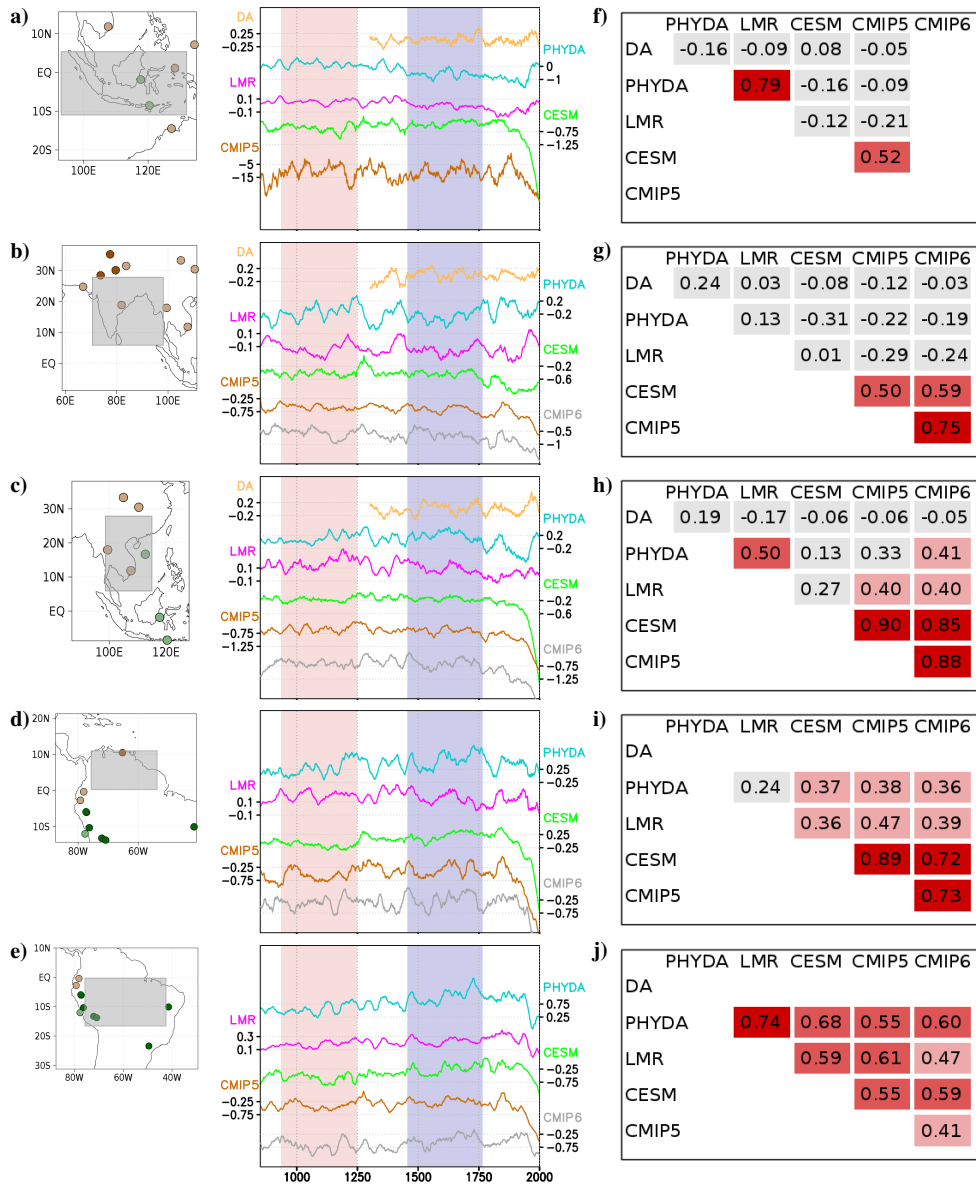


Figure 8. Same as Fig. 7 for (a,f) Indonesia, (b,g) India, (c,h) Southeast Asia, (d,i) northern South America and (e,j) central South America. Time series of DAs are not available for those regions not considered in OWDA, NADA, MADA and MXDA. Time series of CMIP6 are not available for Indonesia, since most CMIP6 simulations do not provide the necessary variables to compute the PDSI for this region.

205 The correlation between the DAs and PHYDA is significant for western North America, while the correlation between the PHYDA and LMR is significant for central South America, northwestern North America, southwestern Europe, Pakistan, Southeast Asia and Indonesia. Some of these correlations exceed 0.7 and are clearly visible in the time series of PDSI from



these regions. This is the case for the correlation between the DA and the PHYDA in southwestern North America (Fig. 7a,f), and the correlation between PHYDA and LMR in Pakistan (Fig. 7d,i), Indonesia (Fig. 8a,f) and central South America (Fig. 8e,j). Regions showing high correlations between reconstruction-based products are in general those regions showing the largest hydroclimate changes during the LM, like those around the ITCZ (Yan et al., 2015; Anchukaitis and Tierney, 2013), those in the Monsoon region (Fleitmann et al., 2003) and in the area of influence of the NAM (Ortega et al., 2015).

Significant correlations are also found between the ensemble averages of CESM-LME, CMIP5 and CMIP6 for regions of South America, India and Southeast Asia, between CMIP5 and CMIP6 ensembles for areas of southeastern Europe, East Africa and Pakistan, and between CESM-LME and CMIP5 ensembles in areas of southwestern Europe and Indonesia. As for the case of reconstruction-based products, some of these correlations exceed 0.7 and are visible in the time series of PDSI, like those of northern South America (Fig. 8d,i) and Southeast Asia (Fig. 8c,h) for CESM-LME, CMIP5 and CMIP6, and those of East Africa (Fig. 7e,j) and India (Fig. 8b,g) for CMIP5 and CMIP6. In these cases, similarities are found during the whole millennium, including a trend in the 20th century not found in the reconstructions (Ljungqvist et al., 2016). The correlation between simulated products is particularly high for those areas with a larger impact of external forcing, like the Atlantic ITCZ (Roldán-Gómez et al., 2020), consistent with the fact that the use of the ensemble average emphasizes the forcing signal (Fernández-Donado et al., 2013; Roldán-Gómez et al., 2020).

Considering this, the comparison between time series from reconstruction-based products and from model simulations would be only relevant for those areas where the contribution of the forcing dominates. Significant correlations are found between the ensemble average of CESM-LME, CMIP5 and CMIP6 LM simulations and the PHYDA and LMR in northern and central South America and, to a lower extent, in regions of southwestern Europe, northern North America and Southeast Asia, suggesting a relevant contribution of the forcing to the hydroclimate of these areas. Some of these correlations between reconstruction-based products and model simulations exceed 0.5 and are visible in the time series of PDSI, like those in central South America (Fig. 8e,j) and those between the LMR and the ensemble average of CMIP5 in southwestern Europe (Fig. 7c,h). These results can be then linked to a particularly important contribution of the forcing in these regions, present in both proxy data and model simulations.

3.4 Correlation between distant regions

As described in the previous sections, distant regions showed similar hydroclimate behaviors during the MCA and LIA. These similarities suggest the presence of coordinated changes between distant regions that go beyond these two periods. To analyse these changes, correlations between the time series of different regions from Fig. 7 and 8 have been computed for the PHYDA (Fig. 9a) and the LMR (Fig. 9b). Both reconstruction-based products show significant positive and negative correlations between distant regions, some of them in agreement with the behavior of reconstructions during the MCA and LIA (Fig. 1).

In particular, both the PHYDA and the LMR show significant negative correlations between central South America and the regions of East Africa and Pakistan. These correlations can be linked to coordinated changes of the Atlantic ITCZ and the monsoon system, in line with those observed in model simulations and associated with shifts of the Atlantic ITCZ in

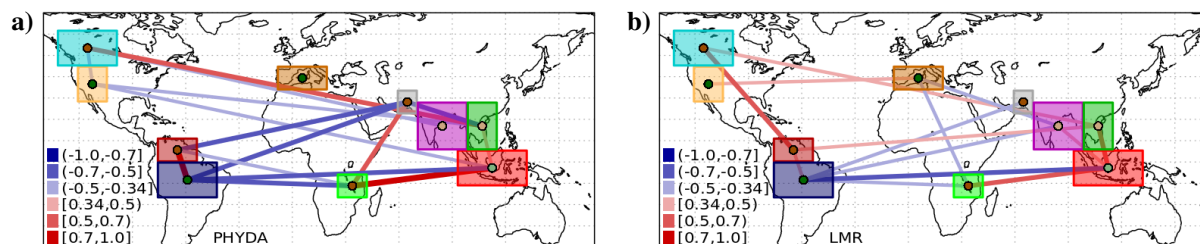


Figure 9. Correlations between time series of PDSI for different regions (solid lines), obtained from (a) PHYDA and (b) LMR. Only significant correlations ($p < 0.05$; $|r| > 0.34$) accounting for autocorrelation are shown, following the color code in the bottom left side of the panels. The color of the points for each region indicate whether the LIA was wetter (green) or drier (brown) than the MCA in the reconstructions of Fig. 1.

response to changes in the external forcing (Roldán-Gómez et al., 2020, 2022). Both reconstruction-based products also show significant positive correlations across the Indian and Pacific basins, such as those between Indonesia and East Africa, and between Southeast Asia and northwestern North America, consistent with the changes in the Pacific Walker circulation found
245 in simulations (Yan et al., 2015).

The correlations across the Pacific basin are emphasized in the PHYDA, which also shows significant negative correlations between southwestern North America and the regions in India and Indonesia. In contrast, the LMR tends to emphasize the variability in the Atlantic basin, with positive correlations between southwestern North America and southwestern Europe following the pattern of the NAO. The spatial correlations found in the PHYDA and LMR are mainly driven by the model used
250 for the data assimilation. However, the fact that the PHYDA and LMR respectively emphasize the variability in the Pacific and Atlantic basin shows that the regional variability given by the proxies is consistent with the spatial patterns from the models. This increases the confidence on the ability of the models to reproduce the behavior of the hydroclimate at a global scale, in particular for those areas and those mechanisms more impacted by the external forcing.

4 Conclusions

255 The analysis of different reconstruction-based and model-based products shows consistent coordinated changes during the LM in the hydroclimate of distant regions. The areas more impacted by these changes are those around the ITCZ, like northern and central South America, East Africa and the Indo-Pacific, those in the area of influence of the NAM/NAO, like western North America and Western Europe, and those of the Indian Monsoon region, extending from the Middle East to Southeast Asia. Even if these changes are particularly important during the MCA and the LIA, for which a high number of reconstructions
260 show drier or wetter conditions, significant correlations between distant regions are also found when considering the whole millennium.

The agreement between reconstruction-based and model-based products for areas of South America and East Africa is indicative of a relevant contribution of the forcing in these regions, consistent with the shifts of the Atlantic ITCZ obtained



in simulations in response to the forcing (Roldán-Gómez et al., 2022). Agreement is also high in the Indian Monsoon region,
265 consistent with an alteration of the monsoon system as a consequence of changes in the forcing (Roldán-Gómez et al., 2020).
A certain agreement is also found for areas of western North America and Western Europe, consistent with an alteration
of the NAM/NAO in response to changes in the forcing (Roldán-Gómez et al., 2020), even if the different products show
discrepancies at regional scales. These discrepancies may be linked to the contribution of internal variability in these areas, but
also to uncertainties in the reconstructed data, limitations in the physics of the models and inaccuracies in the assessment of
270 external forcing considered for the simulations. The largest discrepancies between reconstructed and simulated products are
found in the Indo-Pacific basin, suggesting that this area is more impacted by internal variability processes than by changes in
the forcing.

The combination of reconstructions, model simulations and hybrid products is a powerful technique to overcome the limita-
tions of each individual source. On one hand, the sparse hydroclimate records available from proxy data can be completed with
275 gridded information of atmospheric dynamics and hydroclimate variables provided by model simulations and hybrid products
to extend the analysis to areas not fully covered by the proxies. On the other hand, the representativity of the mechanisms
found in simulations, often involving temperatures, atmospheric dynamics and hydroclimate, like the shifts of the ITCZ, the
alteration of variability modes like the NAM/NAO and the changes in the Walker circulation during the MCA and LIA, could
be confirmed with the hydroclimate information obtained from proxy data and hybrid products.

280 In this work, we considered an exhaustive and up-to-date compilation of all the available reconstruction-based and model-
based sources to analyse the hydroclimate of the LM at a global scale, with a particular focus on the MCA and LIA as periods
with particular forcing conditions. This exercise, perhaps more typical in the analysis of temperatures but systematically applied
for the first time to the global hydroclimate, provided a novel assessment of global hydroclimate changes. The focus on the
MCA and LIA periods and the comparison with model simulations allowed the isolation of those mechanisms potentially
285 impacted by the forcing, while the novel approach based on combining reconstruction-based and model-based sources showed
a coherence in the large-scale changes of the hydroclimate of the LM.

Appendix A: Impact of the definition of the MCA and LIA

For the analyses described in the previous sections, the periods of the MCA and LIA have been respectively defined from 950
to 1250 CE and from 1450 to 1850 CE. This definition may depend on the product and is not applicable at a global scale
290 (Neukom et al., 2014, 2019). For example, reconstructions of the Indo-Pacific basin (Fig. 1, light brown and light green) tend
to show stable conditions only during the early LIA, until late 1500s CE, rather than during the whole LIA as found in regions
of Europe and North America (Fig. 1, dark brown and dark green). To make the analyses independent from the particular
selection of periods for the MCA and LIA, the differences LIA-MCA of Fig. 2 and Fig. 4 have been replaced in Fig. A1 and
Fig. A2 by the slope of PDSI computed over the the whole period from 950 to 1750 CE. The results obtained with this method
295 show no major differences with respect to those shown in Fig. 2 and Fig. 4, confirming that the conclusions obtained in the
paper are independent from the particular definition of the MCA and LIA.

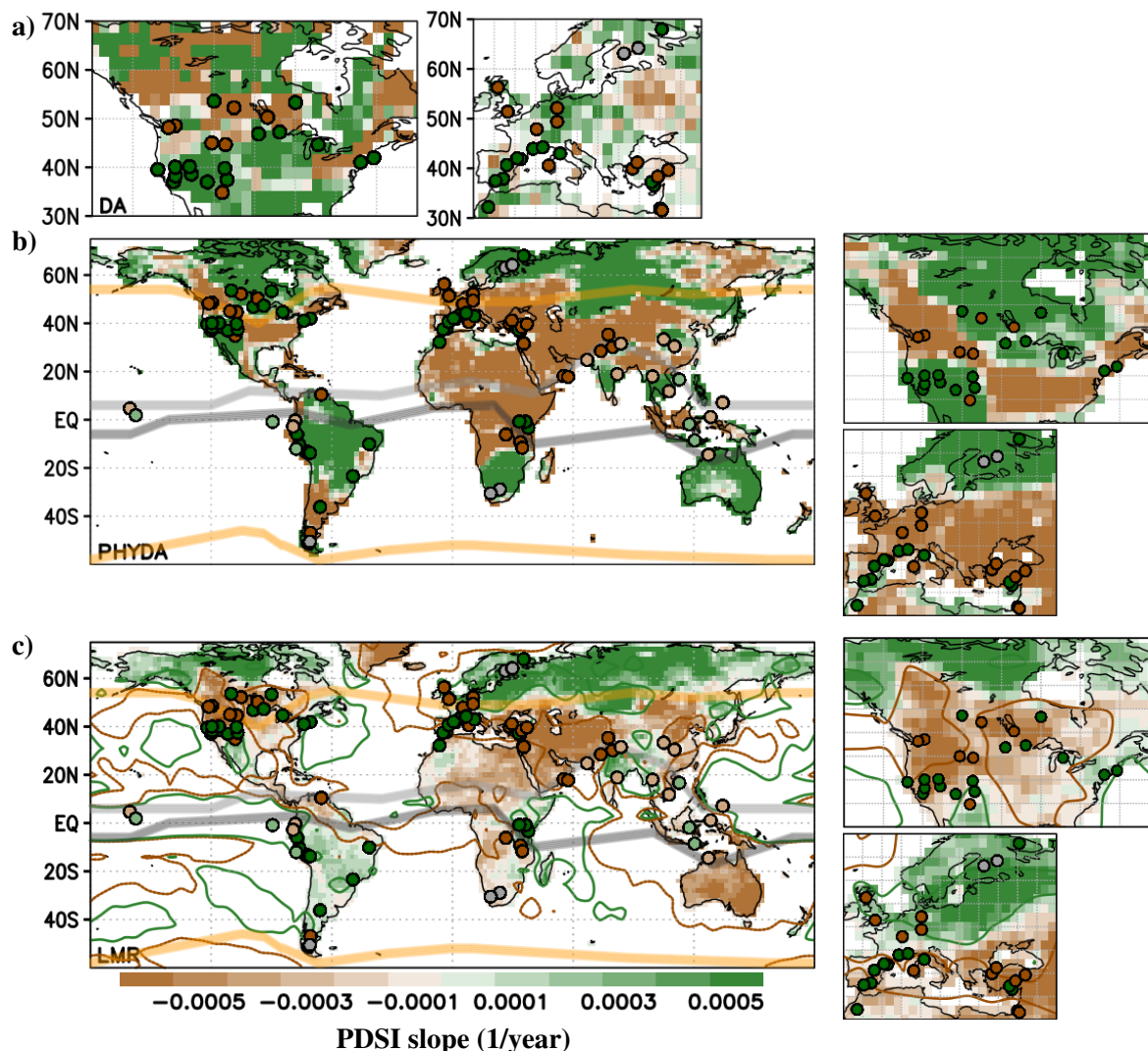


Figure A1. Slope of PDSI (shading) or precipitation (contours) from (a) DAs, (b) PHYDA, and (c) LMR, obtained with a linear regression for the period 950-1750 CE. Dots represent the locations of Fig. 1, with the same color code considered in that figure; positions of the modern ITCZ and NAM and SAM boundaries are also shown, as described in Fig. 1. For the slope of precipitation, contours of -0.001 (brown) and 0.001 (green) mm/month/year are shown. Average of JJA is considered for the PHYDA and the DAs, while the annual average is considered for the LMR. For the PHYDA and the LMR, regional maps over North America and Europe are shown on the right side of each corresponding panel.

Appendix B: Seasonal changes in the PDSI

In the results presented in the previous sections, the JJA PDSI values from the DAs, the PHYDA and the simulations from CESM-LME, CMIP5 and CMIP6 are compared with the annual PDSI provided by the LMR. To confirm that the use of

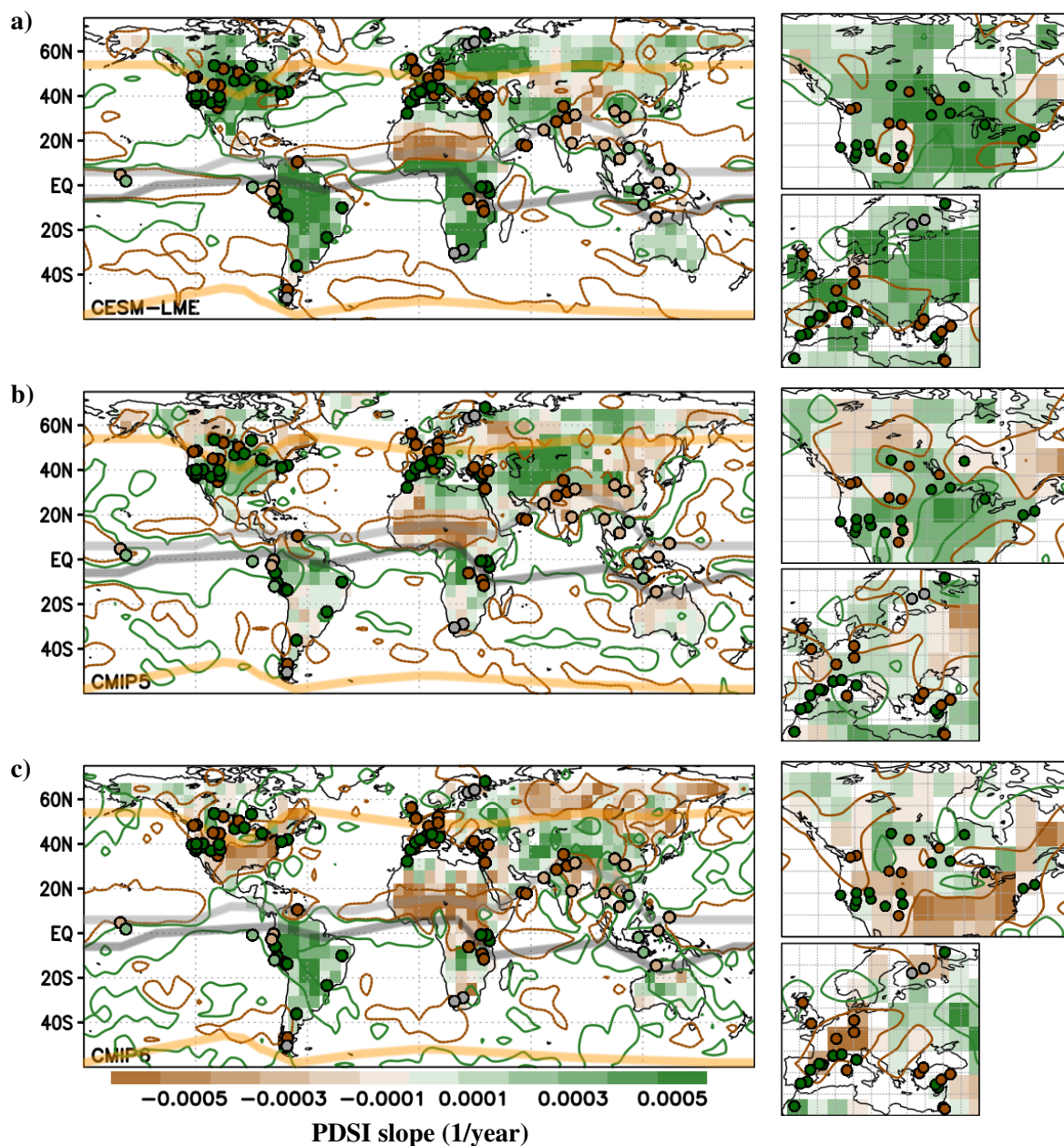


Figure A2. Slope of PDSI (shading) or precipitation (contours) from the ensemble average of (a) CESM-LME, (b) CMIP5 and (c) CMIP6 LM simulations, obtained with a linear regression for the period 950-1750 CE. Dots represent the locations of Fig. 1, with the same color code considered in that figure; positions of the modern ITCZ and NAM and SAM boundaries are also shown, as described in Fig. 1. For the slope of precipitation, contours of -0.001 (brown) and 0.001 (green) mm/month/year are shown. In all the cases, average of JJA is considered. For each product, regional maps over North America and Europe are shown on the right side of each corresponding panel.

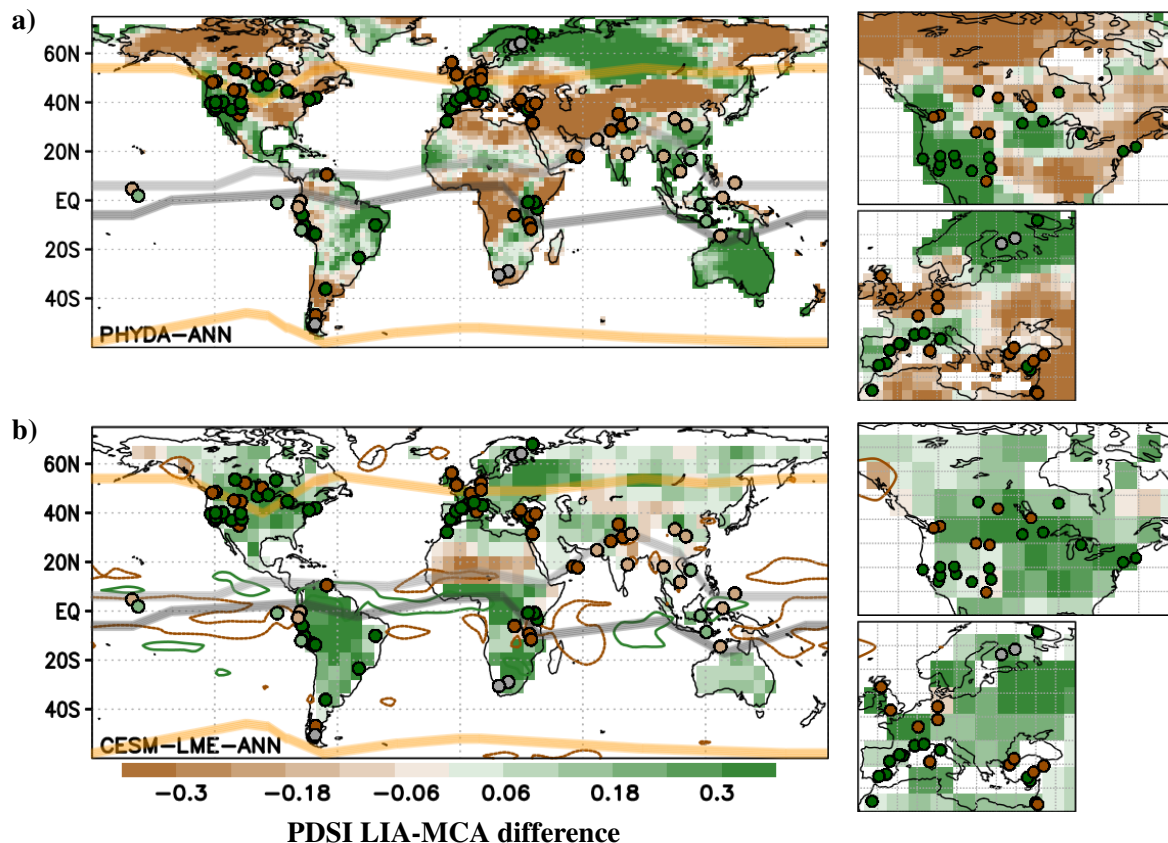


Figure B1. LIA-MCA differences in PDSI (shading) or precipitation (contours) from (a) PHYDA and (b) the ensemble average of CESM-LME, considering annual averages. Dots represent the locations of Fig. 1, with the same color code considered in that figure; positions of the modern ITCZ and NAM and SAM boundaries are also shown, as described in Fig. 1. For the precipitation, contours of -1 (brown) and 1 (green) mm/month are shown. For each case, regional maps over North America and Europe are shown on the right side of each corresponding panel.

300 different averaging periods does not have a significant impact on the results, the annual PDSI from the PHYDA and the
different ensembles of simulations have been also analysed. The difference between the LIA and MCA for the annual PDSI of
of the PHYDA and the ensembles of CESM-LME, CMIP5 and CMIP6 is respectively shown in Fig. B1a, Fig. B1b, Fig. B2a and
Fig. B2b. When comparing these results with those obtained with the average of JJA (Fig. 2b and Fig. 4) only minor differences
are observed, mostly limited to regional scales. This shows that despite the relevant seasonal changes found in the atmospheric
305 variables, the cumulative behavior of the PDSI makes it less sensitive to the season.

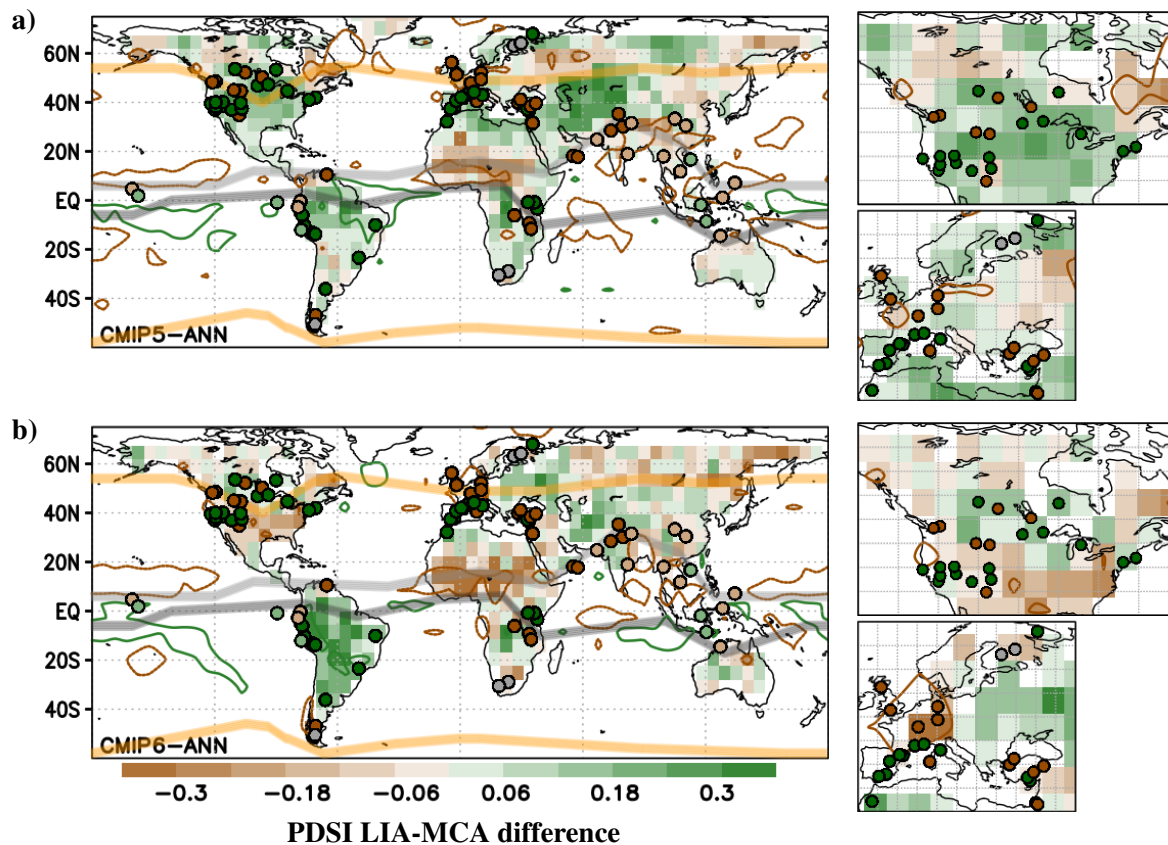


Figure B2. LIA-MCA differences in PDSI (shading) or precipitation (contours) from the ensemble average of (a) CMIP5 and (b) CMIP6 LM simulations, considering annual averages. Dots represent the locations of Fig. 1, with the same color code considered in that figure; positions of the modern ITCZ and NAM and SAM boundaries are also shown, as described in Fig. 1. For the precipitation, contours of -1 (brown) and 1 (green) mm/month are shown. For each case, regional maps over North America and Europe are shown on the right side of each corresponding panel.

Author contributions. This study is part of PJRG's PhD. PJRG contributed with data processing, analysis of results and writing of the paper. JFGR, JES and FGP contributed to the analysis and discussion of results and to writing the paper.

Competing interests. The authors declare that they have no conflict of interest.



Acknowledgements. We gratefully acknowledge the SMILEME (PID2021-126696OB-C21) project. JES was supported in part by the US
310 National Science Foundation grants OISE-1743738 and AGS-2101214. FGP was funded by a FPI contract (PRE2019-090694) of the Spanish
Ministry of Science and Innovation.



References

- Adachi, Y., Yukimoto, S., Deushi, M., Obata, A., Nakano, H., Tanaka, T. Y., Hosaka, M., Sakami, T., Yoshimura, H., Hirabara, M., Shindo, E., Tsujino, H., Mizuta, R., Yabu, S., Koshiro, T., Ose, T., and Kitoh, A.: Basic performance of a new earth system model of the Meteorological Research Institute (MRI-ESM1), *Papers in Meteorology and Geophysics*, 64, 1–19, 2013.
- Anchukaitis, K. J. and Tierney, J. E.: Identifying coherent spatiotemporal modes in time-uncertain proxy paleoclimate records, *Clim. Dyn.*, 41, 1291–1306, 2013.
- Anderson, D. M., Overpeck, J. T., and Gupta, A. K.: Increase in the Asian southwest monsoon during the past four centuries, *Science*, 297, 596–599, 2002.
- Anderson, L.: Holocene record of precipitation seasonality from lake calcite $\delta 18\text{O}$ in the central Rocky Mountains, United States, *Geology*, 39, 211–214, 2011.
- Antonioli, F., Silenzi, S., Gabellini, M., and Mucedda, M.: High resolution climate trend over the last 1000 years from a stalagmite in Sardinia (Italy), *Quat., Nova* 7, 1–5, 2003.
- Apaéstegui, J., Cruz, F. W., Sifeddine, A., Vuille, M., Espinoza, J. C., Guyot, J. L., Khodri, M., Strikis, N., Santos, R. V., Cheng, H., Edwards, L., Carvalho, E., and Santini, W.: Hydroclimate variability of the northwestern Amazon Basin near the Andean foothills of Peru related to the South American Monsoon System during the last 1600 years, *Clim. Past*, 10, 1967–1981, 2014.
- Atwood, A. R., Battisti, D. S., Wu, E., Frierson, D. M. W., and Sachs, J. P.: Data-Model Comparisons of Tropical Hydroclimate Changes Over the Common Era, *Paleoceanography and Paleoclimatology*, 36, e2020PA003 934, 2021.
- Benito, G., Rico, M., Sánchez-Moya, Y., Sopena, A., Thorndycraft, V. R., and Barriendos, M.: The impact of late Holocene climatic variability and land use change on the flood hydrology of the Guadalentín River, southeast Spain, *Global Planet. Change*, 70, 53–63, 2010.
- Benito, G., Thorndycraft, V. R., Rico, M., Sánchez-Moya, Y., Sopena, A., Botero, B. A., Machado, M. J., and Pérez-González, A.: Hydrological response of a dryland ephemeral river to southern African climatic variability during the last millennium, *Quat. Res.*, 75, 471–482, 2011.
- Benson, L., Kashgarian, M., Rye, R., Lund, S., Paillet, F., Smoot, J., Kester, C., Mensing, S., Meko, D., and Lindstrom, S.: Holocene multidecadal and multicentennial droughts affecting northern California and Nevada, *Quat. Sci. Rev.*, 21, 659–682, 2002.
- Berkelhammer, M., Sinha, A., Mudelsee, M., Cheng, H., Edwards, R. L., and Cannariato, K.: Persistent multidecadal power of the Indian Summer Monsoon, *Earth Planet. Sci. Lett.*, 290, 166–172, 2010.
- Bird, B. W., Abbott, M. B., Rodbell, D. T., and Vuille, M.: Holocene tropical South American hydroclimate revealed from a decadal resolved lake sediment $\delta 18\text{O}$ record, *Earth Planet. Sci. Lett.*, 310, 192–202, 2011.
- Bookman, R., Enzel, Y., Agnon, A., and Stein, M.: Late Holocene lake-levels of the Dead Sea, *Bull. Geol. Soc. Am.*, 116, 555–571, 2004.
- Booth, R. K., Notaro, M., Jackson, S. T., and Kutzbach, J. E.: Widespread drought episodes in the western Great Lakes region during the past 2000 years: geographic extent and potential mechanisms, *Earth Planet. Sci. Lett.*, 242, 415–427, 2006.
- Boucher, E., Guiot, J., and Chapron, E.: A millennial multi-proxy reconstruction of summer PDSI for Southern South America, *Clim. Past*, 7, 957–974, 2011.
- Brown, E. T. and Johnson, T. C.: Coherence between tropical East African and South American records of the Little Ice Age, *Geochem. Geophys. Geosyst.*, 6, Q12 005, 2005.
- Bryson, R. and Swain, A.: Holocene variations of monsoon rainfall in Rajasthan, *Quatern. Res.*, 16, 135–145, 1981.



- Buckley, B. M., Palakit, K., Duangsathaporn, K., Sanguantham, P., and Prasomsin, P.: Decadal scale droughts over northwestern Thailand over the past 448 years: Links to the tropical Pacific and Indian Ocean sectors, *Clim. Dynam.*, 29, 63–71, 2007.
- 350 Buckley, B. M., Anchukaitis, K., Penny, D., Fletcher, R., Cook, E. R., Sano, M., Nam, L. C., Wichienkeeo, A., Minh, T. T., and Hong, T. M.: Climate as a contributing factor in the demise of Angkor, Cambodia, *Proc. Natl. Acad. Sci.*, 107, 6748–6752, 2010.
- Büntgen, U., Trouet, V., Frank, D., Leuschner, H. H., Friedrichs, D., Luterbacher, J., and Esper, J.: Tree-ring indicators of German summer drought over the last millennium, *Quat. Sci. Rev.*, 29, 1005–1016, 2010.
- Büntgen, U., Tegel, W., Nicolussi, K., McCormick, M., Frank, D., Trouet, V., Kaplan, J. O., Herzig, F., Heussner, K., Wanner, H., Luterbacher, J., and Esper, J.: 2500 years of european climate variability and human susceptibility, *Science*, 331, 578–582, 2011.
- 355 Burns, S. J., Fleitmann, D., Mudelsee, M., Neff, U., Matter, A., and Mangini, A.: A 780-year annually resolved record of Indian Ocean monsoon precipitation from a speleothem from south Oman, *J. Geophys. Res. Atmos.*, 107, 2002.
- Case, R. A. and MacDonald, G. M.: Tree ring reconstructions of streamflow for three Canadian prairie rivers, *J. Am. Water Resour. Assoc.*, 39, 703–716, 2003.
- 360 Chepstow-Lusty, A. J., Frogley, M. R., Bauer, B. S., Leng, M. J., Boessenkool, K. P., Carcaillet, C., Ali, A. A., and Gioda, A.: Putting the rise of the Inca Empire within a climatic and land management context, *Clim. Past*, 5, 375–388, 2009.
- Coats, S., Smerdon, J. E., Cook, B. I., and Seager, R.: Stationarity of the tropical pacific teleconnection to North America in CMIP5/PMIP3 model simulations, *Geophys. Res. Lett.*, 40, 1–6, 2013a.
- Coats, S., Smerdon, J. E., Seager, R., Cook, B. I., and González-Rouco, J. F.: Megadroughts in Southwestern North America in ECHO-G millennial simulations and their comparison to proxy drought reconstructions, *Am. Met. Soc.*, 26, 7635–7649, 2013b.
- 365 Cook, B. I., Smerdon, J. E., Cook, E. R., Williams, A. P., Anchukaitis, K. J., Mankin, J. S., Allen, K., Andreu-Hayles, L., Ault, T. R., Belmecheri, S., Coats, S., Coulthard, B., Fosu, B., Grierson, P., Griffin, D., Herrera, D. A., Ionita, M., Lehner, F., Leland, C., Marvel, K., Morales, M. S., Mishra, V., Ngoma, J., Nguyen, H. T. T., O’Donnell, A., Palmer, J., Rao, M. P., Rodriguez-Caton, M., Seager, R., Stahle, D. W., Stevenson, S., Thapa, U. K., Varuolo-Clarke, A. M., and Wise, E. K.: Megadroughts in the Common Era and the Anthropocene, *Nature Reviews Earth And Environment*, 3, 741–757, 2022.
- 370 Cook, E. R., Woodhouse, C. A., Eaking, C. M., Meko, D. M., and Stahle, D. W.: Long-term aridity changes in the western United States, *Science*, 306, 1015–1018, 2004.
- Cook, E. R., Anchukaitis, K. J., Buckley, B. M., D’Arrigo, R. D., Jacoby, G. C., and Wright, W. E.: Asian Monsoon Failure and Megadrought During the Last Millennium, *Science*, 328, 486–489, 2010a.
- 375 Cook, E. R., Seager, R., Heim, R. R., Vose, R. S., Herweijer, C., and Woodhouse, C.: Megadroughts in North America: placing IPCC projections of hydroclimatic change in a long-term palaeoclimate context, *J. Quat. Sci.*, 25, 48–61, 2010b.
- Cook, E. R., Seager, R., Kushnir, Y., Briffa, K., Buntgen, U., Frank, D., Krusic, P., Tegel, W., van der Schrier, G., Andreu-Hayles, L., Baillie, M., Baittinger, C., Bleicher, N., Bonde, N., Brown, D., Carrer, M., Cooper, R., Cufar, K., Dittmar, C., Esper, J., Griggs, C., Gunnarson, B., Gunther, B., Gutierrez, E., Haneca, K., Helama, S., Herzig, F., Heussner, K.-U., Hofmann, J., Janda, P., Kontic, R., Kose, N., Kyncl, T., 380 Levanic, T., Linderholm, H., Manning, S., Melvin, T. M., Miles, D., Neuwirth, B., Nicolussi, K., Nola, P., Panayotov, M., Popa, I., Rothe, A., Seftigen, K., Seim, A., Svarva, H., Svoboda, M., Thun, T., Timonen, M., Touchan, R., Trotsiuk, V., Trouet, V., Walder, F., Wazny, T., Wilson, R., and Zang, C.: Old World megadroughts and pluvials during the Common Era, *Science Advances*, 1, 1500561, 2015.
- Denniston, R. F., Ummenhofer, C. C., Jr., A. D. W., Lachniet, M. S., Villarini, G., Asmerom, Y., Polyak, V. J., Passaro, K. J., Cugley, J., Woods, D., and Humphreys, W. F.: Expansion and Contraction of the Indo-Pacific Tropical Rain Belt over the Last Three Millennia, 385 *Scientific Reports*, 6, 34485, 2016.



- Diaz, H. F., Trigo, R., Hughes, M. K., Mann, M. E., Xoplaki, E., and Barriopedro, D.: Spatial and temporal characteristics of climate in Medieval Times revisited, *Bull. Am. Meteorol. Soc.*, 92, 1487–1500, 2011.
- Dufresne, J., Foujols, M., Denvil, S., Caubel, A., Marti, O., Aumont, O., Balkanski, Y., Bekki, S., Bellenger, H., Benschila, R., Bony, S., Bopp, L., Braconnot, P., Brockmann, P., Cadule, P., Cheruy, F., Codron, F., Cozic, A., Cugnet, D., de Noblet, N., Duvel, J., Ethe, C., Fairhead, L., Fichet, T., Flavoni, S., Friedlingstein, P., Grandpeix, J., Guez, L., Guilyardi, E., Hauglustaine, D., Hourdin, F., Idelkadi, A., Ghattas, J., Joussaume, S., Kageyama, M., Krinner, G., Labetoulle, S., Lahellec, A., Lefebvre, M., Lefevre, F., Levy, C., Li, Z. X., Lloyd, J., Lott, F., Madec, G., Mancip, M., Marchand, M., Masson, S., Meurdesoif, Y., Mignot, J., Musat, I., Parouty, S., Polcher, J., Rio, C., Schulz, M., Swingedouw, D., Szopa, S., Talandier, C., Terray, P., Viovy, N., and Vuichard, N.: Climate change projections using the IPSL-CM5 Earth System Model: From CMIP3 to CMIP5, *Climate Dyn.*, 40, 2123–2165, 2013.
- 390 Ely, L. L., Enzel, Y., Baker, V. R., and Cayan, D. R.: A 5000-year record of extreme floods and climate change in the southwestern United States, *Science*, 262, 410–412, 1993.
- Esper, J., Frank, D., Büntgen, U., Verstege, A., Luterbacher, J., and Xoplaki, E.: Long-term drought severity variations in Morocco, *Geophys. Res. Lett.*, 34, L17 702, 2007.
- Eyring, V., Bony, S., Meehl, G. A., Senior, C. A., Stevens, B., Stouffer, R. J., and Taylor, K. E.: Overview of the Coupled Model Intercomparison Project Phase 6 (CMIP6) experimental design and organization, *Geosci. Model Dev.*, 9, 1937–1958, 2016.
- 400 Fernández-Donado, L., González-Rouco, J. F., Raible, C. C., Ammann, C. M., Barriopedro, D., García-Bustamante, E., Jungclauss, J. H., Lorenz, S. J., Luterbacher, J., Phipps, S. J., Servonnat, J., Swingedouw, D., Tett, S. F. B., Wagner, S., Yiou, P., and Zorita, E.: Large-scale temperature response to external forcing in simulations and reconstructions of the last millennium, *Clim. Past*, 9, 393–421, 2013.
- Fleitmann, D., Burns, S. J., Mudelsee, M., Neff, U., Kramers, J., Mangini, A., and Matter, A.: Holocene forcing of the Indian monsoon recorded in a stalagmite from Southern Oman, *Science*, 300, 1737–1739, 2003.
- 405 Fogt, R. L., Perlwitz, J., Monaghan, A. J., Bromwich, D. H., Jones, J. M., and Marshall, G. J.: Historical SAM variability. Part II: Twentieth-Century variability and trends from reconstructions, observations, and the IPCC AR4 models, *Am. Met. Soc.*, 2009.
- Garcin, Y., Williamson, D., Taieb, M., Vincens, A., Mathe, P. E., and Majule, A.: Centennial to millennial changes in maar-lake deposition during the last 45,000 years in tropical Southern Africa (Lake Masoko, Tanzania), *Palaeogeogr. Palaeoclimatol. Palaeoecol.*, 239(3-4), 334–354, 2006.
- 410 Garcin, Y., Williamson, D., Bergonzini, L., Radakovitch, O., Vincens, A., Buchet, G., Guiot, J., Brewer, S., Mathé, P., and Majule, A.: Solar and anthropogenic imprints on Lake Masoko (southern Tanzania) during the last 500 years, *J. Paleolimnol.*, 37, 475–490, 2007.
- Gilbert, E., Bergonzini, L., Massault, M., and Williamson, D.: AMS-C14 chronology of 40.0 cal ka BP continuous deposits from a crater lake (Lake Masoko, Tanzania) - modern water balance and environmental implications, *Palaeogeogr. Palaeoclimatol. Palaeoecol.*, 187(3-4), 307–322, 2002.
- 415 Giorgetta, M. A., Jungclauss, J., Reick, C. H., Legutke, S., Bader, J., Böttinger, M., Brovkin, V., Crueger, T., Esch, M., Fieg, K., Glushak, K., Gayler, V., Haak, H., Hollweg, H., Ilyina, T., Kinne, S., Kornbluh, L., Matei, D., Mauritsen, T., Mikolajewicz, U., Mueller, W., Notz, D., Pithan, F., Raddatz, T., Rast, S., Redler, R., Roeckner, E., Schmidt, H., Schnur, R., Segschneider, J., Six, K. D., Stockhause, M., Timmreck, C., Wegner, J., Widmann, H., Wieners, K., Claussen, M., Marotzke, J., and Stevens, B.: Climate and carbon cycle changes from 1850 to 2100 in MPI ESM simulations for the Coupled Model Intercomparison Project phase 5, *J. Adv. Model. Earth Syst.*, 5, 572–597, 2013.
- Göktürk, O. M.: Climate in the Eastern Mediterranean through the Holocene inferred from Turkish stalagmites, Ph.D. thesis, University of Bern, p. 113 pp, 2011.



- Göktürk, O. M., Fleitmann, D., Badertscher, S., Cheng, H., Edwards, R. L., and Tüysüz, O.: Climate on the Southern Black Sea coast during the Holocene: implications from the Sofular Cave record, *Quat. Sci. Rev.*, 30, 2433–2445, 2011.
- 425 Gong, D. Y. and Wang, S. W.: Definition of Antarctic Oscillation Index, *Geophys. Res. Lett.*, 26, 459–462, 1999.
- Graham, N. E., Hughes, M. K., Ammann, C. M., Cobb, K. M., Hoerling, M. P., Kennett, D. J., Kennett, J. P., Rein, B., Stott, L., Wigand, P. E., and Xu, T.: Tropical Pacific - mid-latitude teleconnections in medieval times, *Clim. Change*, 83, 241–285, 2007.
- Graham, N. E., Ammann, C. M., Fleitmann, D., Cobb, K. M., and Luterbacher, J.: Support for global climate reorganization during the "Medieval Climate Anomaly", *Clim. Dyn.*, 2010.
- 430 Gray, S. T., Fastie, C. L., Jackson, S. T., and Betancourt, J. L.: Tree-ring based reconstruction of precipitation in the Bighorn Basin, Wyoming, since 1260 AD, *J. Climate*, 17, 3855–3865, 2004.
- Greenbaum, N., Schick, A. P., and Baker, V. R.: The palaeoflood record of a hyperarid catchment, Nahal Zin, Negev Desert, Israel, *Earth Surf. Process. Landforms*, 25, 951–971, 2000.
- Griffiths, M. L., Kimbrough, A. K., Gagan, M. K., Drysdale, R. N., Cole, J. E., Johnson, K. R., Zhao, J. X., Cook, B. I., Hellstrom, J. C., and
435 Hantoro, W. S.: Western Pacific hydroclimate linked to global climate variability over the past two millennia, *Nature Communications*, 7, 11 719, 2016.
- Grissino-Mayer, H. D.: Tree-ring reconstructions of climate and fire history at El Malpais National Monument, New Mexico, Ph.D. dissertation. The University of Arizona, p. 407 pp, 1995.
- Gupta, A., Anderson, D., and Overpeck, J.: Abrupt changes in the Asian southwest monsoon during the Holocene and their links to the North
440 Atlantic Ocean, *Nature*, 421, 354–357, 2003.
- Hajima, T., Watanabe, M., Yamamoto, A., Tatebe, H., Noguchi, M. A., Abe, M., Ohgaito, R., Ito, A., Yamazaki, D., Okajima, H., Ito, A., Takata, K., Ogochi, K., Watanabe, S., and Kawamiya, M.: Development of the MIROC-ES2L Earth system model and the evaluation of biogeochemical processes and feedbacks, *Geosci. Model Dev.*, 13, 2197–2244, 2020.
- Haug, G. H., Hughen, K. A., Sigman, D. M., Peterson, L. C., and Röhl, U.: Southward migration of the intertropical convergence zone
445 through the Holocene, *Science*, 293, 1304–1308, 2001.
- Helama, S., Meriläinen, J., and Tuomenvirta, H.: Multicentennial megadrought in northern Europe coincided with a global El Niño–Southern Oscillation drought pattern during the Medieval Climate Anomaly, *Geology*, 37, 175–178, 2009.
- Higley, M. C., Conroy, J. L., and Schmitt, S.: Last millennium meridional shifts in hydroclimate in the central tropical Pacific, *Paleoceanography and Paleoclimatology*, 33, 354–366, 2018.
- 450 Hu, C., Henderson, G. M., Huang, J., Xie, S., Sun, Y., and Johnson, K. R.: Quantification of Holocene Asian monsoon rainfall from spatially separated cave records, *Earth and Planetary Science Letters*, 266, 221–232, 2008.
- Hughes, M. K. and Funkhouser, G.: Extremes of moisture availability reconstructed from tree rings for recent millennia in the Great Basin of western North America. In: *The Impacts of Climate Variability on Forests*, Springer, New York, pp. 99–107, 1998.
- Johnson, T. and McCave, I.: Transport mechanism and paleoclimatic significance of terrigenous silt deposited in varved sediments of an
455 African rift lake, *Limnol. Oceanogr.*, 53(4), 1622–1632, 2008.
- Johnson, T. C., Barry, S. L., Chan, Y., and Wilkinson, P.: Decadal record of climate variability spanning the past 700 yr in the Southern Tropics of East Africa, *Geology*, 29(1), 83–86, 2001.
- Jones, J. M., Fogt, R. L., Widmann, M., Marshall, G. J., Jones, P. D., and Visbeck, M.: Historical SAM variability. Part I: Century-Length seasonal reconstructions, *Am. Met. Soc.*, 2009.



- 460 Jones, M. D., Roberts, N., Leng, M. J., and Türke, M.: A high-resolution late Holocene lake isotope record from Turkey and links to North Atlantic and monsoon climate, *Geology*, 34(5), 361–364, 2006.
- Jungclauss, J. H., Bard, E., Baroni, M., Braconnot, P., Cao, J., Chini, L. P., Egorova, T., Evans, M., González-Rouco, J. F., Goosse, H., Hurtt, G. C., Joos, F., Kaplan, J. O., Khodri, M., Goldewijk, K. K., Krivova, N., LeGrande, A. N., Lorenz, S. J., Luterbacher, J., Man, W., Maycock, A. C., Meinshausen, M., Moberg, A., Muscheler, R., Nehrbass-Ahles, C., Otto-Bliesner, B. I., Phipps, S. J., Pongratz, J.,
465 Rozanov, E., Schmidt, G. A., Schmidt, H., Schmutz, W., Schurer, A., Shapiro, A. I., Sigl, M., Smerdon, J. E., Solanki, S. K., Timmreck, C., Toohey, M., Usoskin, I. G., Wagner, S., Wu, C., Yeo, K. L., Zanchettin, D., Zhang, Q., and Zorita, E.: The PMIP4 contribution to CMIP6 - Part 3: The last millennium, scientific objective, and experimental design for the PMIP4 past1000 simulations, *Geosci. Model Dev.*, 10, 4005–4033, 2017.
- Kremenetski, K. V., Boettger, T., and Vaschalova, G. M. M., Sulerzhitsky, L., and Hiller, A.: Medieval climate warming and aridity as
470 indicated by multiproxy evidence from the Kola Peninsula, Russia, *Palaeogeography, Palaeoclimatology, Palaeoecology*, 209, 113–125, 2004.
- Kuzucuoglu, C., Dörfler, W., Kunesch, S., and Goupille, F.: Mid- to late-Holocene climate change in central Turkey: the Tecer Lake record, *Holocene*, 21, 173–188, 2011.
- Laird, K. R., Fritz, S. C., Grimm, E. C., and Mueller, P. G.: Century-scale paleoclimatic reconstruction from Moon Lake, a closed-basin lake
475 in the northern Great Plains, *Limnol. Oceanogr.*, 41(5), 890–902, 1996.
- Laird, K. R., Haig, H. A., Ma, S., Kingsbury, M. V., Brown, T. A., Lewis, C. F. M., Oglesby, R. J., and Cumming, B. F.: Expanded spatial extent of the Medieval Climate Anomaly revealed in lake-sediment records across the boreal region in northwest Ontario, *Global Change Biol.*, 18, 2869–2881, 2012.
- Landrum, L., Otto-Bliesner, B., Wahl, E., Conley, A., Lawrence, P., Rosenbloom, N., and Teng, H.: Last Millennium Climate and its Variability in CCSM4, *Journal of Climate*, 1, 1085–1111, 2013.
- Langton, S. J., Linsley, B. K., Robinson, R. S., Rosenthal, Y., Oppo, D. W., Eglinton, T. I., Howe, S. S., Djajadihardja, Y. S., and Syamsudin, F.: 3,500 yr record of centennial-scale climate variability from the Western Pacific Warm Pool, *Geology*, 36, 795–798, 2008.
- Ledru, M. P., Jomelli, V., Samaniego, P., Vuille, M., Hidalgo, S., Herrera, M., and Ceron, C.: The Medieval Climate Anomaly and the Little Ice Age in the eastern Ecuatorian Andes, *Clim. Past*, 9, 307–321, 2013.
- 485 Li, J. and Wang, J.: A modified zonal index and its physical sense, *Geophys. Res. Lett.*, 30, doi: 10.1029/2003GL017441, 2003.
- Ljungqvist, F. C., Krusic, P. J., Sundqvist, H. S., Zorita, E., Brattström, G., and Frank, D.: Northern Hemisphere hydroclimate variability over the past twelve centuries, *Nature*, 532, 94–98, 2016.
- Llasat, D. C. M., Rigo, T., and Barriendos, M.: The 'Montserrat-2000' flash-flood event: A comparison with the floods that have occurred in the northeastern Iberian Peninsula since the 14th century, *Int. J. Climatol.*, 23, 453–469, 2003.
- 490 Luoto, T. P., Helama, S., and Nevalainen, L.: Stream flow intensity of the Saavanjoki River, eastern Finland, during the past 1500 years reflected by mayfly and caddisfly mandibles in adjacent lake sediments, *J. Hydrol.*, 476, 147–153, 2013.
- Luterbacher, J., García-Herrera, R., Akcer-On, S., Allan, R., Alvarez-Castro, M. C., Benito, G., Booth, J., Büntgen, U., Cagatay, N., Colombaroli, D., Davis, B., Esper, J., Felis, T., Fleitmann, D., Frank, D., Gallego, D., Garcia-Bustamante, E., Glaser, R., Gonzalez-Rouco, F., Goosse, H., Kiefer, T., Macklin, M. G., Manning, S. W., Montagna, P., Newman, L., Power, M. J., Rath, V., Ribera, P., Riemann, D.,
495 Roberts, N., Sicre, M. A., Silenzi, S., Tinner, W., Tzedakis, P. C., Valero-Garcés, B., Schrier, G., Vannièrè, B., Vogt, S., Wanner, H., Werner, J. P., Willett, G., Williams, M. H., Xoplaki, E., Zerefos, C. S., and Zorita, E.: A review of 2000 years of paleoclimatic evidence in the Mediterranean. In: *The Climate of the Mediterranean Region: From the Past to the Future*, Elsevier, 1, 87–185, 2012.



- Magny, M., de Beaulieu, J. L., Drescher-Schneider, R., Vanniere, B., Walter-Simonnet, A. V., Miras, Y., Millet, L., Bossuet, G., Peyron, O., Brugiapaglia, E., and Leroux, A.: Holocene climate changes in the central Mediterranean as recorded by lake-level fluctuations at Lake
500 Accesa (Tuscany, Italy), *Quat. Sci. Rev.*, 26, 1736–1758, 2007.
- Mann, M. E., Zhang, Z., Rutherford, S., Bradley, R. S., Hughes, M. K., Shindell, D., Ammann, C., Faluvegi, G., and Ni, F.: Global signatures and dynamical origins of the Little Ice Age and Medieval Climate Anomaly, *Science*, 326, 1256–1260, 2009.
- Martín-Puertas, C., Valero-Garcés, B. L., Mata, P., González-Sampériz, P., Bao, R., and Moreno, A.: Arid and humid phases in Southern Spain during the last 4000 years: the Zoñar Lake record, *Córdoba, Holocene*, 18, 907–921, 2008.
- 505 Martín-Puertas, C., Jiménez-Espejo, F., Martínez-Ruiz, F., Nieto-Moreno, V., Rodrigo, M., and Mata, M. P.: Late Holocene climate variability in the southwestern Mediterranean region: an integrated marine and terrestrial geochemical approach, *Clim. Past*, 6, 807–816, 2010.
- Masson-Delmotte, V., Schulz, M., Abe-Ouchi, A., Beer, J., Ganopolski, A., Rouco, J. F. G., Jansen, E., Lambeck, K., Luterbacher, J., Naish, T., Osborn, T., Otto-Bliesner, B., Quinn, T., Ramesh, R., Rojas, M., Shao, X., and Timmermann, A.: Information from Paleoclimate Archives. In: *Climate Change 2013: The Physical Science Basis. Contribution of Working Group I to the Fifth Assessment Report of the*
510 *Intergovernmental Panel on Climate Change*, Cambridge University Press, 2013.
- Mauritsen, T., Bader, J., Becker, T., Behrens, J., Bittner, M., Brokopf, R., Brovkin, V., Claussen, M., Crueger, T., Esch, M., Fast, I., Fiedler, S., Fläschner, D., Gayler, V., Giorgetta, M., Goll, D. S., Haak, H., Hagemann, S., Hedemann, C., Hohenegger, C., Ilyina, T., Jahns, T., de-la Cuesta, D. J., Jungclaus, J., Kleinen, T., Kloster, S., Kracher, D., Kinne, S., Kleberg, D., Lasslop, G., Kornbluh, L., Marotzke, J., Matei, D., Meraner, K., Mikolajewicz, U., Modali, K., Möbis, B., Müller, W. A., Nabel, J. E. M. S., Nam, C. C. W., Notz, D., Nyawira, S. S.,
515 Paulsen, H., Peters, K., Pincus, R., Pohlmann, H., Pongratz, J., Popp, M., Raddatz, T. J., Rast, S., Redler, R., Reick, C. H., Rohrschneider, T., Schemann, V., Schmidt, H., Schnur, R., Schulzweida, U., Six, K. D., Stein, L., Stemmler, I., Stevens, B., von Storch, J. S., Tian, F., Voigt, A., Vrese, P., Wieners, K. H., Wilkenskjaeld, S., Winkler, A., and Roeckner, E.: Developments in the MPI-M Earth System Model version 1.2 (MPI-ESM1.2) and its response to increasing CO₂, *Journal of Advances in Modeling Earth Systems*, 11, 998–1038, 2019.
- Meko, D. M., Therrell, M. D., Baisan, C. H., and Hughes, M. K.: Sacramento River flow reconstructed to AD 869 from tree rings, *J. Amer.*
520 *Water Resour. Assoc.*, 37, 1029–1039, 2001.
- Michels, A., Laird, K. R., Wilson, S. E., Thomson, D., Leavitt, P. R., Oglesby, R. J., and Cumming, B. F.: Multidecadal to millennial-scale shifts in drought conditions on the Canadian Prairies over the past six millennia: Implications for future drought assessment, *Global Change Biol.*, 13(7), 1295–1307, 2007.
- Morellón, M., Valero-Garcés, B., Vegas-Vilarrúbia, T., González-Sampériz, P., Romero, O., Delgado-Huertas, A., Moreno, P. M. A., Rico, M., and Corella, J. P.: Late glacial and Holocene palaeohydrology in the western Mediterranean region: the Lake Estanya record (NE
525 Spain), *Quat. Sci. Rev.*, 28, 2582–2599, 2009.
- Morellón, M., Valero-Garcés, B. L., González-Sampériz, P., Vegas-Vilarrúbia, T., Rubio, E., Rieradevall, M., Delgado-Huertas, A., Mata, P., Romero, O., Engstrom, D. R., López-Vicente, E., Navas, A., and Soto, J.: Climate changes and human activities recorded in the sediments of Lake Estanya (NE Spain) during the Medieval Warm Period and Little Ice Age, *J. Paleolimnol.*, 46, 423–452, 2011.
- 530 Moreno, A., Valero-Garcés, B., Gonzales-Sampériz, P., and Rico, M.: Flood response to rainfall variability during the last 2000 years inferred from the Taravilla Lake record (Central Iberian Range, Spain), *J. Paleolimnol.*, 40, 943–961, 2008.
- Moy, C. M., Seltzer, G. O., Rodbell, D. T., and Anderson, D. M.: Variability of El Niño/Southern Oscillation activity at millennial timescales during the Holocene epoch, *Nature*, 420, 162–165, 2002.
- Neukom, R., Luterbacher, J., Villalba, R., Kuettel, M., Frank, D., Jones, P. D., Grosjean, M., Esper, J., Lopez, L., and Wanner, H.: Multi-
535 centennial summer and winter precipitation variability in southern South America, *Geophys. Res. Lett.*, 37, L14 708, 2010.



- Neukom, R., Gergis, J., Karoly, D. J., Wanner, H., Curran, M., Elbert, J., González-Rouco, F., Linsley, B. K., Moy, A. D., Mundo, I., Raible, C. C., Steig, E. J., van Ommen, T., Vance, T., Villalba, R., Zinke, J., and Frank, D.: Inter-hemispheric temperature variability over the past millennium, *Nature Climate Change*, 4, 362–367, 2014.
- Neukom, R., Steiger, N., Gómez-Navarro, J. J., Wang, J., and Werner, J. P.: No evidence for globally coherent warm and cold periods over
540 the preindustrial Common Era, *Nature*, 571, 550–554, 2019.
- Neumann, F. H., Kagan, E. J., Schwab, M. J., and Stein, M.: Palynology, sedimentology and palaeoecology of the late Holocene Dead Sea, *Quat. Sci. Rev.*, 26, 1476–1498, 2007.
- Newton, A., Thunell, R., and Stott, L.: Climate and hydrographic variability in the Indo-Pacific Warm Pool during the last millennium, *Geophys. Res. Lett.*, 33, L19710, 2006.
- 545 Novello, V. F., Cruz, F. W., Karmann, I., Burns, S. J., Strikis, N. M., Vuille, M., Cheng, H., Edwards, R. L., Barreto, E. A. S., and Frigo, E.: Multidecadal climate variability in Brazil’s Nordeste during the last 3000 years based on speleothem isotope records, *Geophys. Res. Lett.*, 39, L23706, 2012.
- Ortega, P., Lehner, F., Swingedouw, D., Masson-Delmotte, V., Raible, C. C., Casado, M., and Yiou, P.: A model-tested North Atlantic Oscillation reconstruction for the past millennium, *Nature*, 523, 71–74, 2015.
- 550 Oswald, W. W. and Foster, D. R.: A record of late-Holocene environmental change from southern New England, USA, *Quat. Res.*, 76, 314–318, 2011.
- Otto-Bliesner, B. L., Brady, E. C., Fasullo, J., Jahn, A., Landrum, L., Stevenson, S., Rosenbloom, N., Mai, A., and Strand, G.: Climate variability and change since 850 C.E.: An ensemble approach with the Community Earth System Model (CESM), *Bull. Am. Meteorol. Soc.*, 2015.
- 555 Palmer, W.: Meteorologic drought, U.S. Weather Bureau, Res. Pap. No. 45, 58, 1965.
- Pederson, D. C., Peteet, D. M., Kurdyla, D., and Guilderson, T.: Medieval Warming, Little Ice Age, and European impact on the environment during the last millennium in the lower Hudson Valley, New York, USA, *Quat. Res.*, 63, 238–249, 2005.
- Phadtare, N. and Pant, R.: A century-scale pollen record of vegetation and climate history during the past 3500 years in the Pinder Valley, Kumaon Higher Himalaya, *J. Geol. Soc. India*, 68, 495–506, 2006.
- 560 Phipps, S., Rotstayn, L., Gordon, H., Roberts, J., Hirst, A., and Budd, W.: The CSIRO Mk3L climate system model version 1.0 - Part 2: Response to external forcings, *Geosci. Model Dev.*, 5, 649–682, 2012.
- Proctor, C. J., Baker, A., Barnes, W. L., and Gilmour, M.: A thousand year speleotherm proxy record of North Atlantic climate from Scotland, *Clim. Dyn.*, 16, 815–820, 2000.
- Rein, B., Lückge, A., and Sirocko, F.: A major Holocene ENSO anomaly during the Medieval period, *Geophys. Res. Lett.*, 31, L17211,
565 2004.
- Reuter, J., Stott, L., Khider, D., Sinha, A., Cheng, H., and Edwards, R. L.: A new perspective on the hydroclimate variability in northern South America during the Little Ice Age, *Geophys. Res. Lett.*, 36, L21706, 2009.
- Roldán-Gómez, P. J., González-Rouco, J. F., Melo-Aguilar, C., and Smerdon, J. E.: Dynamical and hydrological changes in climate simulations of the last millennium, *Clim. Past*, 16, 1285–1307, 2020.
- 570 Roldán-Gómez, P. J., González-Rouco, J. F., Melo-Aguilar, C., and Smerdon, J. E.: The Role of Internal Variability in ITCZ Changes Over the Last Millennium, *Geophys. Res. Lett.*, 49, e2021GL096487, 2022.
- Routson, C. C., Woodhouse, C. A., and Overpeck, J. T.: Second century megadrought in the Rio Grande headwaters, Colorado: How unusual was medieval drought?, *Geophys. Res. Lett.*, 38, L22703, 2011.



- Sachs, J. P., Sachse, D., Smittenberg, R. H., Zhang, Z. H., Battisti, D. S., and Golubic, S.: Southward movement of the Pacific intertropical convergence zone AD 1400–1850, *Nature Geosci.*, 2, 519–525, 2009.
- Schmidt, G., Ruedy, R., Hansen, J., Aleinov, I., Bell, N., Bauer, M., Bauer, S., Cairns, B., Canuto, V., Cheng, Y., Genio, A. D., Faluvegi, G., Friend, A., Hall, T., Hu, Y., Kelley, M., Kiang, N., Koch, D., Lacis, A., Lerner, J., Lo, K., Miller, R., Nazarenko, L., Oinas, V., Perlwitz, J., Perlwitz, J., Rind, D., Romanou, A., Russell, G., Sato, M., Shindell, D., Stone, P., Sun, S., Tausnev, N., Thresher, D., , and Yao, M.: Present day atmospheric simulations using GISS ModelE: Comparison to in-situ, satellite and reanalysis data, *J. Climate*, 19, 153–192, 2006.
- Schmidt, G., Kelley, M., Nazarenko, L., Ruedy, R., Russell, G., Aleinov, I., Bauer, M., Bauer, S., Bhat, M., Bleck, R., Canuto, V., Chen, Y., Cheng, Y., Clune, T., Genio, A. D., de Fainchtein, R., Faluvegi, G., Hansen, J., Healy, R., Kiang, N., Koch, D., Lacis, A., LeGrande, A., Lerner, J., Lo, K., Matthews, E., Menon, S., Miller, R., Oinas, V., Olosa, A., Perlwitz, J., Puma, M., Putman, W., Rind, D., Romanou, A., Sato, M., Shindell, D., Sun, S., Syed, R., Tausnev, N., Tsigaridis, K., Unger, N., Voulgarakis, A., Yao, M., and Zhang, J.: Configuration and assessment of the GISS ModelE2 contributions to the CMIP5 archive, *J. Adv. Model. Earth Syst.*, 6, 141–184, 2014.
- Schmidt, G. A., Jungclaus, J. H., Ammann, C. M., Bard, E., Braconnot, P., Crowley, T., Delaygue, G., Joos, F., Krivova, N. A., Muscheler, R., Otto-Bliesner, B. L., Pongratz, J., Shindell, D. T., Solanki, S. K., Steinhilber, F., and Vieira, L. E. A.: Climate forcing reconstructions for use in PMIP simulations of the Last Millennium (v1.0), *Geosci. Model Dev.*, 4, 33–45, 2011.
- Schmidt, G. A., Jungclaus, J. H., Ammann, C. M., Bard, E., Braconnot, P., Crowley, T., Delaygue, G., Joos, F., Krivova, N. A., Muscheler, R., Otto-Bliesner, B. L., Pongratz, J., Shindell, D. T., Solanki, S. K., Steinhilber, F., and Vieira, L. E. A.: Climate forcing reconstructions for use in PMIP simulations of the Last Millennium (v1.1), *Geosci. Model Dev.*, 5, 185–191, 2012.
- Schurer, A. P., Hegerl, G. C., Mann, M. E., Tett, S. F. B., and Phipps, S. J.: Separating forced from chaotic climate variability over the past millennium, *J. Climate*, 26, 6954–6973, 2013.
- Sheffer, N. A., Rico, M., Enzel, Y., Benito, G., and Grodek, T.: The palaeoflood record of the Gardon river, France: A comparison with the extreme 2002 flood event, *Geomorphology*, 10.1016, 2007.
- Sinha, A., Cannariato, K. G., Stott, L. D., Cheng, H., Edwards, R. L., Yadava, M. G., Ramesh, R., and Singh, L. B.: A 900-year (600 to 1500 A.D.) record of the Indian summer monsoon precipitation from the core monsoon zone of India, *Geophys. Res. Lett.*, 34, 2007.
- Smerdon, J. E., Cook, B. I., Cook, E. R., and Seager, R.: Bridging Past and Future Climate across Paleoclimatic Reconstructions, Observations, and Models: A Hydroclimate Case Study, *Journal of Climate*, 28, 3212–3231, 2015.
- Stager, J. C., Ryves, D., Cumming, B. F., Meeker, L. D., and Beer, J.: Solar variability and the levels of Lake Victoria, East Africa, during the last millenium, *J. Paleolimnol.*, 33, 243–251, 2005.
- Stahle, D. W., Cook, E. R., Burnette, D. J., Villanueva, J., Cerano, J., Burns, J. N., Griffin, D., Cook, B. I., Acuna, R., Torbenson, M. C. A., Szejner, P., and Howard, I. M.: The Mexican Drought Atlas: Tree-ring reconstructions of the soil moisture balance during the late pre-Hispanic, colonial, and modern eras, *Quaternary Science Reviews*, 149, 34–60, 2016.
- Steiger, N. J., Smerdon, J. E., Cook, E. R., and Cook, B. I.: A reconstruction of global hydroclimate and dynamical variables over the Common Era, *Scientific Data*, 5, 180086, 2018.
- Steinman, B. A., Abbott, M. B., Mann, M. E., Stansell, N. D., and Finney, B. P.: 1,500 year quantitative reconstruction of winter precipitation in the Pacific Northwest, *Proc. Natl. Acad. Sci.*, 109, 11 619–11 623, 2013.
- Stevens, L. R. and Dean, W. E.: Geochemical evidence for hydroclimatic variability over the last 2,460 years from Crevice Lake in Yellowstone National Park, USA, *Quat. Int.*, 188, 139–148, 2008.



- St. George, S. and Nielsen, E.: Hydroclimatic change in southern Manitoba since A. D. 1409 inferred from tree rings, *Quat. Res.*, 58, 103–111, 2002.
- Stine, S.: Extreme and persistent drought in California and Patagonia during mediaeval time, *Nature*, 369, 546–549, 1994.
- Stocker, T. F., Qin, D., Plattner, G. K., Alexander, L. V., Allen, S. K., Bindoff, N. L., Bréon, F. M., Church, J. A., Cubasch, U., Emori, S.,
615 Forster, P., Friedlingstein, P., Gillett, N., Gregory, J. M., Hartmann, D. L., Jansen, E., Kirtman, B., Knutti, R., Kumar, K. K., Lemke, P.,
Marotzke, J., Masson-Delmotte, V., Meehl, G. A., Mokhov, I. I., Piao, S., Ramaswamy, V., Randall, D., Rhein, M., Rojas, M., Sabine,
C., Shindell, D., Talley, L. D., Vaughan, D. G., and Xie, S. P.: Technical Summary. In: *Climate Change 2013: The Physical Science
Basis. Contribution of Working Group I to the Fifth Assessment Report of the Intergovernmental Panel on Climate Change*, Cambridge
University Press, 2013.
- 620 Tardif, R., Hakim, G. J., Perkins, W. A., Horlick, K. A., Erb, M. P., Emile-Geay, J., Anderson, D. M., Steig, E. J., and Noone, D.: Last
Millennium Reanalysis with an expanded proxy database and seasonal proxy modeling, *Clim. Past*, 15, 1251–1273, 2019.
- Taylor, B. L.: A speleothems-based high resolution reconstruction of climate in southeastern Brazil over the past 4,100 years, M.S. thesis,
University of Massachusetts, 2010.
- Taylor, C. M., Parker, D. J., and Harris, P. P.: An observational case study of mesoscale atmospheric circulations induced by soil moisture,
625 *Geophys. Res. Lett.*, 34, L15 801, 2007.
- Tett, S., Betts, R., Crowley, T., Timothy, J., Johns, C., Jones, A., Osborn, T., Öström, E., Roberts, D., and Woodage, M.: The impact of natural
and anthropogenic forcings on climate and hydrology since 1550, *Clim. Dynam.*, 28, 3–34, 2007.
- Thompson, D. W. J. and Wallace, J. M.: Regional Climate Impacts of the Northern Hemisphere Annular Mode, *Science*, 293, 85–89, 2001.
- Thompson, L. G., Mosley-Thompson, E., Dansgaard, W., and Grootes, P. M.: The Little Ice Age as recorded in the stratigraphy of the tropical
630 Quelccaya Ice Cap, *Science*, 234, 361–364, 1986.
- Thorntwaite, C. W.: An approach toward a rational classification of climate, *Geogr. Rev.*, 38, 55–94, 1948.
- Tierney, J., Mayes, M., Meyer, N., Johnson, C., Swarzenski, P., Cohen, A., and Russell, J.: Late-twentieth-century warming in Lake Tan-
ganyika unprecedented since AD 500, *Nature Geosci.*, 3(6), 422–425, 2010a.
- Tierney, J. E., Oppo, D. W., Rosenthal, Y., Russell, J. M., and Linsley, B. K.: Coordinated hydrological regimes in the Indo-Pacific region
635 during the past two millennia, *Paleoceanography*, 25, PA1102, 2010b.
- Touchan, R., Akkemik, U., Hughes, M. K., and Erkan, N.: May-June precipitation reconstruction of southwestern Anatolia, Turkey during
the last 900 years from tree rings, *Quat. Res.*, 68, 196–202, 2007.
- Treydte, K., Schleser, G. H., Helle, G., Frank, D. C., Winiger, M., Haug, G. H., and Esper, J.: The twentieth century was the wettest period
in northern Pakistan over the past millennium, *Nature*, 440, 1179–1182, 2006.
- 640 Tyson, P. D. and Lindsay, J. A.: The climate of the last 2000 years in southern Africa, *The Holocene*, 2, 271–278, 1992.
- Verschuren, D.: Reconstructing fluctuations of a shallow East African lake during the past 1800 yrs from sediment stratigraphy in a submerged
crater basin, *J. Paleolimnol.*, 25(3), 297–311, 2001.
- Verschuren, D., Laird, K., and Cumming, B.: Rainfall and drought in equatorial East Africa during the past 1000 years, *Nature*, 403, 410–414,
2000.
- 645 Verschuren, D., Damste, J. S. S., Moernaut, J., Kristen, I., Blaauw, M., Fagot, M., and Haug, G. H.: Half-precessional dynamics of monsoon
rainfall near the East African Equator, *Nature*, 462, 637–641, 2009.
- von Rad, U., Schaaf, M., Michels, K. H., Schulz, H., Berger, W. H., and Sirocko, F.: A 5000-yr record of climate change in varved sediments
from the oxygen minimum zone of Pakistan, northeastern Arabian Sea, *Quatern. Res.*, 51, 39–53, 1999.



- 650 Vuille, M., Burns, S. J., Taylor, B. L., Cruz, F. W., Bird, B. W., Abbott, M. B., Kanner, L. C., Cheng, H., and Novello, V. F.: A review of the South American Monsoon history as recorded in stable isotopic proxies over the past two millennia, *Clim. Past*, 2012.
- Wang, Y., Cheng, H., Edwards, R. L., He, Y., Kong, X., An, Z., Wu, J., Kelly, M. J., Dykoski, C. A., and Li, X.: The Holocene Asian monsoon: links to solar changes and North Atlantic climate, *Science*, 308, 854, 2005.
- 655 Watanabe, S., Hajima, T., Sudo, K., Nagashima, T., Takemura, T., Okajima, H., Nozawa, T., Kawase, H., Abe, M., Yokohata, T., Ise, T., Sato, H., Kato, E., Takata, K., Emori, S., and Kawamiya, M.: MIROC-ESM 2010: model description and basic results of CMIP5-20c3m experiments, *Geosci. Model Dev.*, 4, 845–872, 2011.
- Wells, N., Goddard, S., and Hayes, M. J.: A self-calibrating Palmer Drought Severity Index, *Journal of Climate*, 17, 2335–2351, 2004.
- Wilhelm, B., Arnaud, F., Sabatier, P., Crouzet, C., Brisset, E., Chaumillon, E., Disnar, J., Guiter, F., Malet, E., Reyss, J., Tachikawa, K., Bard, E., and Delannoy, J.: 1400 years of extreme precipitation patterns over the Mediterranean French Alps and possible forcing mechanisms, *Quat. Res.*, 78, 1–12, 2012.
- 660 Wilson, R. J. S., Miles, D., Loader, N., Melvin, T. M., Cunningham, L., Cooper, R. J., and Briffa, K. R.: A millennial long March–July precipitation reconstruction for southern-central England, *Clim. Dyn.*, 40, 997–1017, 2012.
- Wolff, C., Haug, G. H., Timmermann, A., Damste, J. S. S., Brauer, A., Sigman, D. M., Cane, M. A., and Verschuren, D.: Reduced interannual rainfall variability in east Africa during the Last Ice Age, *Science*, 333, 743–747, 2011.
- 665 Woodbridge, J. and Roberts, N.: Late Holocene climate of the Eastern Mediterranean inferred from diatom analysis of annually-laminated lake sediments, *Quat. Sci. Rev.*, 30, 3381–3392, 2011.
- Yan, H., Sun, L., Oppo, D. W., Wang, Y., Liu, Z., Xie, Z., Liu, X., and Cheng, W.: South China Sea hydrological changes and Pacific Walker Circulation variations over the last millennium, *Nature Communications*, 2, 293, 2011.
- Yan, H., Wei, W., Soon, W., An, Z., Zhou, W., Liu, Z., Wang, Y., and Carter, R. M.: Dynamics of the intertropical convergence zone over the western Pacific during the Little Ice Age, *Nature Geosci.*, 8, DOI: 10.1038/NGEO2375, 2015.
- 670 Yukimoto, S., Yoshimura, H., Hosaka, M., Sakami, T., Tsujino, H., Hirabara, M., Tanaka, T. Y., Deushi, M., Obata, A., Nakano, H., Adachi, Y., Shindo, E., Yabu, S., Ose, T., and Kitoh, A.: Meteorological Research Institute - Earth System Model Version 1 (MRI-ESM1) - Model Description, *Tech. Rep. of the Met. Res. Inst.*, 64, 2011.
- Yukimoto, S., Kawai, H., Koshiro, T., Oshima, N., Yoshida, K., Urakawa, S., Tsujino, H., Deushi, M., Tanaka, T., Hosaka, M., Yabu, S., Yoshimura, H., Shindo, E., Mizuta, R., Obata, A., Adachi, Y., and Ishii, M.: The Meteorological Research Institute Earth System Model 675 Version 2.0, MRI-ESM2.0: Description and Basic Evaluation of the Physical Component, *Journal of the Meteorological Society of Japan. Ser. II*, 97, 931–965, 2019.
- Zhang, P. Z., Cheng, H., Edwards, R. L., Chen, F., Wang, Y., Yang, X., Liu, J., Tan, M., Wang, X., Liu, J., An, C., Dai, Z., Zhou, J., Zhang, D., Jia, J., Jin, L., and Johnson, K. R.: A test of climate, sun, and culture relationships from an 1810-year Chinese cave record, *Science*, 322, 940–942, 2008.